Norwegian University of Life Sciences

Master's Thesis 2023 **60 ECTS**

Faculty of Biosciences

Genetic and molecular basis of calcium influence on the production of carotenoids in *Mucor circinelloides*

Ida Emilie Larsen

M.Sc. Genome Science

Preface

This master thesis was developed under the ongoing Earth Biogenome Project (EBP), a non-commercial initiative that has the goal of sequencing and categorizing the genomes of the 1.5 million eukaryotic species on Earth within the next 10 years. EBP Norway (EBP-NOR) is a collaboration between the major universities in Norway (UIO, NMBU, UiB, NTNU, Uni Nord and UiT), SINTEF, and the non-academic institution's REV Ocean, The Life Science Cluster and ArticZymes Technologies. Together the EBP-NOR project will sequence and categorize all eukaryotic species in Norway, estimated to 45 000 species. The laboratory work was executed at NMBU between August 2022 and February 2023.

I would first and foremost like to thank my main supervisor Simen Rød Sandve (Professor), assisting supervisor Volha Shapaval (Associate Professor), and Helle Tessand Baalsrud (Postdoc) for their guidance and support during my thesis, as well as a special thanks to Dana Byrtusova (Postdoc) for all assistance with my lab work. I am very fortunate and grateful to have worked with such a great team both at CIGENE and REALTEK. Lastly, I want to thank my partner, friends and family for all the encouragement and support during this exciting and challenging process.

Ida Emilie Larsen

Sammendrag - Norsk

Karotenoider er høyt verdsatte metabolitter, på grunn av deres mangfoldige, kommersielle bruksområder i mat, fôr og kosmetisk industri. Spesielt karotenoider produsert av sopp er av bioteknologisk interesse på grunn av deres ernæringsmessig egenskaper. I soppceller nøytraliserer karotenoider frie radikaler, og forhindrer dermed oksidativ skade i soppen. *Mucor circinelloides* er en dimorfisk, filamentøs muggsopp, som produserer mange karotenoider som kan brukes i diverse bioteknologiske områder. Tidligere har det blitt påvist at mangel på kalsium fører til økt produksjon av karotenoider i denne arten. Kalsium er aktiv i mange vitale prosesser i sopp, slik som dannelsen av cellevegger, hyfe vekst og stresstoleranse i celler. Kalsium er en ekte sekundær budbringer, som påvirker alle aspektene av en celles livssyklus, inkludert stressresponser og akklimatisering. Man vet foreløpig ikke nøyaktig hvordan kalsiummangel påvirker pigmentproduksjon i *Mucor circinelloides*. For å fylle dette kunnskapshullet trenger man mer kunnskap om den genregulatoriske og molekylære responsen som fører til økt pigmentering i *Mucor circinelloides*. Som en del av det pågående Earth Biogenome prosjektet, ble genomet til *Mucor circinelloides* sekvensert og satt sammen. *Mucor circinelloides* ble kultivert med og uten tilgang til kalsium i vekstmediet. Spektroskopi og kromatografi ble gjort for å kvantifisere karotenoid og fettinnhold ved de ulike behandlingene. Videre ble genuttrykket kvantifisert og analysert for å forstå kalsiums påvirkning på genregulering av produksjon av karotenoider. Vi fant at kalsium påvirker den karotenoidproduserende veien via økt protein syntese, dimorfisk endring, karakterisert av økt gjærvekst og regulering av ulike kandidatgener for produksjon av karotenoider. Flere av genene identifisert i dette studiet har ingen kjent funksjon og videre funksjonelle genetiske studier trengs derfor for å avdekke effekten av kalsium på karotenoider. Dette studiet har bidratt til forståelsen av den genetiske og molekylære påvirkningen av kalsium på karotenoid produksjon, og gitt oss ny kunnskap som er av stor nytte for videre utvikling av industriell pigmentproduksjon i sopp.

Summary - English

Carotenoids are highly valuable metabolites, due to their diverse commercial application in the food, feed, and cosmetics industries. Especially carotenoids produced by fungi are of the biotechnology industry's interest due to their nutraceutical properties. Carotenoids function as neutralizers of free radicals in fungal cells, preventing oxidative damage to the cells. *Mucor circinelloides,* a dimorphic filamentous fungi, produce various carotenoids valuable for the different aspects of biotechnology industries. It has been shown that calcium starvation positively affects carotenoid production in this species.

Calcium is active in many vital processes in fungi, by having an important role in cell wall synthesis, hyphae growth and stress tolerance in the cells. Calcium is also a true second messenger and impacts every aspect of the cell's life cycle, including activating stress response signaling and acclimatization. How calcium affects pigment production in *Mucor circinelloides* has not yet been described. In order to fill this knowledge gap understanding the gene regulatory and molecular response would be essential.

As part of the ongoing Earth Biogenome Project, the genome of *Mucor circinelloides* was sequenced and assembled. Different samples of *Mucor circinelloides* were grown with or without calcium in their growth media. Spectroscopy and chromatography were done to quantify the relative carotenoid and lipid content as a result of different calcium treatments. Gene expression was quantified and analyzed to identify candidate genes affecting the production of carotenoids without calcium. We found that calcium influences the carotenoid biosynthesis both indirectly and directly, through protein synthesis, dimorphic switching (increased yeast-like growth) and regulation of different carotenoid genes. However, many of the genes found to influence carotenoid production are of unknown function, thus functional studies are needed to shed light on the effect of calcium on this trait. This study contributes to the understanding of the genetic and molecular basis of the influence calcium has in the production of carotenoids in *Mucor circinelloides* and will be of immense value to industrial production of carotenoids in this species.

Table of contents

1 Introduction

Carotenoids are a crucial group of natural antioxidants present in a wide range of species. Carotenoids are fat-soluble pigments, known as tetraterpenoids (Ashokkumar et al., 2023), and are extensively utilized in the food, pharmaceutical, and cosmetic industries. Although over 600 carotenoids have been recognized in nature, only a few, namely β-carotene, lutein, lycopene, and astaxanthin, are currently commercially exploited. Chemical synthesis can produce carotenes; however, the preference for naturally produced carotenoids has increased due to the growing concern about artificial food coloring (Iturriaga et al., 2000). Currently, chemically synthesized carotenoids are less expensive than biologically produced ones. The production cost for chemically produced astaxanthin is approximately $1000 per kilo and around $2500-7000 per kilo for biologically produced astaxanthin. β-carotene production by chemical synthesis is expected to be even less expensive since the operating cost for biologically produced β-carotene from *Dunaliella salina* is around $343.54-499,59 (Igreja et al., 2021).
Pigments synthesized by fungi are considered highly valuable metabolites due to their diverse commercial applications as colorants in the food, feed, and cosmetics industries and their nutraceutical properties. Carotenoids function as neutralizers of free radicals in fungal cells, preventing oxidative stress damage to the cells. Carotenoids also decrease membrane fluidity, reducing oxidative damage by controlling oxygen diffusion rate, and serve as metabolic precursors of trisporic acid, which is essential for sexual reproduction (Dzurendova et al., 2021).

Fungal species such as *Mucor circinelloides* and *Blakeslea trispora*, can be used for industrial β-carotene production. β-carotene is a lipophilic carotene, meaning that it tends to accumulate in lipophilic compartments like membranes or lipoproteins, and is a pro-vitamin A (Naz et al., 2020; Tapiero et al., 2004). Both *B. trispora* and *M. circinelloides* have been identified as capable of synthesizing various carotenes, with β-carotene being the most prominent. *B. trispora* is the highest producer of β-carotene and other carotenoids and is frequently used industrially. However, *B. trispora* has limitations associated with industrial use, including a decline in carotenoid accumulation when grown in a shaker and the need for surface cultivation. *M. circinelloides* is more favorable for β-carotene production because it does not require complex fermentation processes and is therefore highly attractive for biotechnological development (Naz et al., 2020).
In one of the latest studies (Dzurendova et al., 2021) it has been shown a considerable effect of calcium cation on lipid and pigment production in oleaginous Mucoromycota fungi. It has been reported that the absence of calcium together with low phosphorus in the media makes some strains of *Mucor circinelloides* produce more carotenoids. The effect of calcium on pigment production in Mucoromycota fungi, like *Mucor circinelloides* has not yet been described. Filling this knowledge gap and understanding the genetic response would be valuable learning for the industry. A high-quality genome sequence as well as information regarding gene regulation under different growth conditions could be utilized to improve carotene-content production in *Mucor circinelloides.*

1.1 Background

1.1.1 *Mucor circinelloides*

Mucor circinelloides is a dimorphic filamentous fungus. As all dimorphic fungi, *Mucor circinelloides* when grown in liquid culture can possess two cell forms - long thin filaments hyphae and single yeast-like cells. Dimorphic growth is known as phase transition and is a fundamental feature of the biology and lifestyle of these fungi. Temperature is the predominant stimulus that influences this transition in phase. When the fungi are grown at 2-25°C it has a hyphae phase. When grown at 37°C it grows into a yeast-like morphology. Other environmental factors influencing this transition include elevated CO_2, exogenous cysteine, and estradiol (Gauthier, 2017). Filamentous growth of *Mucor circinelloides* is performed by apical extension of filaments. When the fungus continues to grow, a complex network of hyphae is made, referred to as mycelium (Powers-Fletcher et al., 2016).

Mucor circinelloides reproduce asexually or sexually. The asexual reproduction is characterized by the formation of sporgangiphores (Botha & Botes, 2014). *Mucor circinelloides* have two types of sporangiophores. One being sympodially branched and the other being elongated (Fazili et al., 2022). Sexual reproduction in *Mucor circinelloides* occurs when two similar gametangia conjugate to produce a zygospore (Botha & Botes, 2014).

Mucor circinelloides is also an oleaginous fungus, meaning it can naturally accumulate a relatively large amount of lipids that can account for up to 20 to 80% (w/w) of biomass. These lipids have a similar fatty acid profile as vegetable oils, where mono- and di-unsaturated fatty acids are dominating. Thus, lipids obtained from *Mucor circinelloides* has a significant nutritional value and can be used as food and feed ingredients, mostly because of essential fatty acids such as gamma-linolenic acid (GLA; 18:3n-6). These lipids are accumulated in organelles called lipid droplets, which are localized intracellularly and closely connected to the endoplasmic reticulum (Dzurendova et al., 2021). This fungus has a versatile metabolism and can be used for single-cell oil production. *Mucor circinelloides* is widely applicable in a range of biotechnological processes, and is well known as a robust cell factory. They have a range of extracellular products including enzymes like cellulases, lipases, proteases, phytases, and amylases, and ethanol. *Mucor circinelloides* can also accumulate and synthesize a range of intracellular components, such as chitosan and chitin, polyphosphates, lipids, and carotenoids (Dzurendova et al., 2020).

Mucor circinelloides belongs to the Kingdom: Fungi, Phylum: Mucoromycota, Order: Mucorales, and the Family Mucoraceae (Fazili et al., 2022). There are a lot of different subspecies and strains of *Mucor circinelloides*. Some of these are *Mucor circinelloides f. circinelloides, Mucor circinelloides f. lusitanicus,* FRR 5020, VI 4770, CBS 277.49 and WJ11.

Even though they are the same species, they display large phenotypic divergence in several key traits. For instance, strain FRR 5020 produces a lot of pigments in stressful environments, whereas strain VI4770 accumulates a lot of lipids under stress, but little to no accumulation of pigments (Dzurendova et al., 2021). *Mucor circinelloides f. circinelloides*, *Mucor circinelloides f. lusitanicus* and *Mucor circinelloides f. griseocyanus* are three different subspecies of *Mucor cirinelloides*. A study from 2014 reveals from whole-genome sequencing comparisons of draft genome assemblies of *M. circinelloides f. lusitanicus* and *M. circinelloides f. circinelloides* genomes, a significant difference in sequence identity by dramatic rearrangements on the genome, including at least six large inversions and a number of regions that were not aligned between the two genomes, suggesting it can be classified as two different species (Lee et al., 2014).

1.1.2 Role of Calcium & Phosphorus in fungal cells

Calcium has long been known to be active in many vital processes in fungi, animals, and plants. Calcium is a true second messenger. In fungi, high levels of calcium are found in cell walls, vacuoles, and most organelles (Moreau, 1987). Some of the cellular processes in fungal cells where calcium is required are nutrient uptake, germination, formation of asexual spores (conidia), and sexual reproduction. Most of the calcium in fungi, as well as plants, is associated with the extracellular milieu (mostly in cell walls) (Moreau, 1987). In eukaryotic cells, calcium is required at the endoplasmic reticulum (ER), where it provides the correct function of protein folding and secretory machinery (Dzurendova et al., 2021).

Calcium plays an important role in cell wall synthesis, as well as hyphae growth and stress tolerance (Dzurendova et al., 2021). Calcium is also a vital second messenger for activating stress response signaling and cell acclimatization in eukaryotic cells, yet calcium's effect on stress is poorly understood due to the lack of effective tools with which to investigate changes both in real-time and at the level of single cells. A study done on dynamic calcium-mediated stress response and recovery signatures in the fungal pathogen, *Candida albicans*, suggested that the cells were able to acclimatize to an increase in osmotic stress when calcium ions are present in the media (Giuraniuc et al., 2023).

In both plant and fungal cells, the highest levels of calcium are found in the vacuoles. Because the concentration of calcium in the cytosol is very low, and the concentration in the organelles and cell walls is high, fungal cells must have efficient mechanisms to maintain the huge concentration gradient (Moreau, 1987). Fungi possess six major types of calcium transporters: Calcium pumps, Calcium/Hydrogen exchangers, high-affinity calcium systems (HACS), low-affinity calcium systems (LACS), TRP-like calcium channels, and mitochondrial calcium uniporter (MCU). Calcium/Hydrogen exchangers are responsible for regulating intracellular pH, whereas HACS and LACS are involved in the regulation of cytosolic calcium levels. TRP-like calcium channels are involved in calcium influx, while MCU is involved in mitochondrial calcium uptake (Roy et al., 2021).

Calcium is capable of precipitating phosphate, which may be lethal to the cell. (Roy et al., 2021). The two fundamental tools of signal transduction are the abilities of calcium ions and phosphate ions to modify local electrostatic fields and protein conformations. These two signaling elements have been shaped by evolution as the primary means of communication within cells, with calcium ions carrying a positive charge (cation) and phosphate ions carrying a negative charge (anion). Calcium signaling impacts every aspect of the cell's life cycle. As the most rigorously regulated ion among all membrane-bound organisms, calcium binds to a multitude of proteins to facilitate changes in localization, association, and function (Clapham, 2007).

1.1.3 Biosynthetic pathway of carotenoids

The biosynthetic pathway for carotenoid production divides into four modules, starting from a carbon source and leading to carotenoids (Figure 1.1). The first model is the central carbon module, here a carbon source is used to make G3P, and then pyruvate. Pyruvate can be used further in the synthesis of acetyl Co-enzyme A (CoA).
The co-factor module is the use of NADPH and ATP in the synthesis of the different compounds in the central carbon module.
In the isoprene supplement module, pyruvate and CoA can be used in two separate pathways producing dimethylallyl diphosphate (DAMPP) and isopentenyl diphosphate (IPP), respectively. The synthesis of IPP requires a vast amount of ATP and begins with the conversion of acetyl CoA to 3-hydroxy-3-methyl glutaryl-CoA (HMG-CoA), catalyzed by HMG-CoA synthase. Then, HMG-CoA is converted into mevalonic acid (MVA), which is the first precursor of the terpenoid biosynthetic pathway. MVA is phosphorylated by MVA kinase and decarboxylation; into isopentenyl pyrophosphate (IPP). IPP can either be hydrolyzed by pyrophosphatases into IP, be in the reversible isomerization to DAMPP, or be used directly in the carotenoid biosynthesis module. The DAMPP pathway does not require as much ATP as the IPP pathway. DAMPP pathway starts with the synthase of 1-deoxy-D-xylulose 5-phosphate (DXP) and ends in the synthesis of 4-hydroxy-3-methylbut-2-en-1-yl diphosphate (HMBPP). HMBPP can either be hydrolyzed into DAMPP or IPP. DAMPP has the possibility to be in the reversible isomerization to IPP or be directly used in the carotenoid biosynthesis module.
The carotenoid biosynthesis module starts with either or both DAMPP and IPP. Two prenyl-transferase reactions are needed to produce C30 carotenoids. With a third prenyl-transferase reaction, geranylgeranyl diphosphate (GGPP) is condensed. This diphosphate can then further be used in the production of C40, C50, and C60 carotenoids (Li et al., 2020).

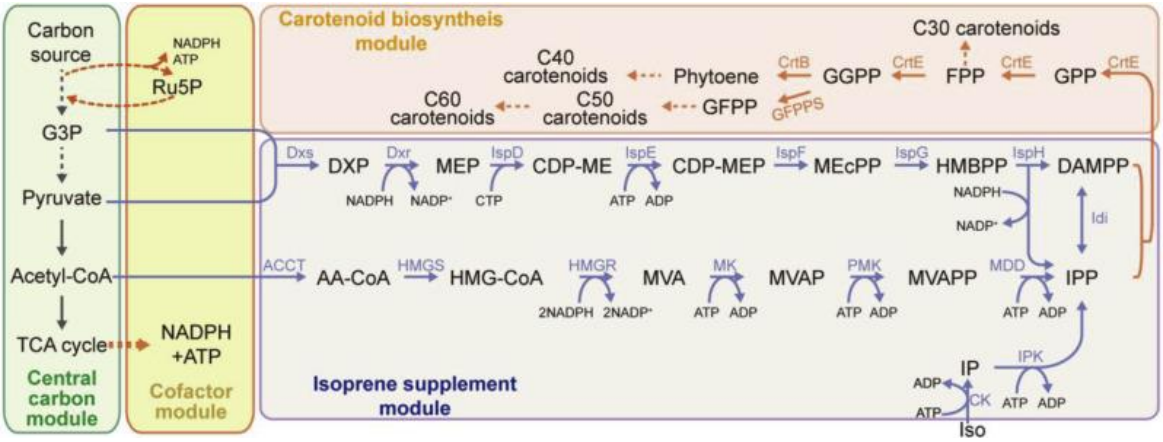

Figure 1.1 Biosynthetic pathway of carotenoids: *Scheme of microbial carotenoid biosynthesis collected from "Modular engineering for microbial production of carotenoids" study (Li et al., 2020) The whole metabolic pathway of carotenoids divides into four modules, starting from a carbon source and leading to carotenoids.*

1.1.4 Genetic basis for carotenoid production

Some genetic studies have been done on carotenoid production in *Mucor circinelloides (reviewed in (Iturriaga et al., 2000)*), resulting in a list of genes putatively involved in the biosynthesis of carotenoids (Iturriaga et al., 2000). These genes are *carB* encoding phytoene dehydrogenase, *carRP* encoding phytoene synthase/lycopene cyclase, *carG* encoding GGPP synthase, and *crgA* encoding a putative transcriptional factor. *carB* and *carRA* are also found in the Mucorales species *Phycomyces blakesleeanus*, encoding the same dehydrogenase and synthase. In a study on the development of a plasmid-free CRISPR-Cas9 system for the genetic modification of *Mucor circinelloides*, they tested the deletion of the genes *carB* (phytoene dehydrogenase) and *hmgR2* (3-hydroxy-3-methylglutaryl-CoA reductase) (Nagy et al., 2017). Colonies in which the targeted *carB* gene was disrupted, had a white color since they were unable to produce the carotenoid, β-carotene. The disruption of the *hmgR2* gene resulted in no change in carotene production, but a decrease in ergosterol content. *Mucor circinelloides* has three different *hmgR* genes (*hmgR1*, *hmgR2* and *hmgR3*). In this study, the results suggested that *hmgR2* did not affect the carotenoid content, but the overlapping function of the two genes (*hmgR2* and *hmgR3*) affected the carotene production and that *hmgR3* has a major role in the carotene biosynthesis.

Gene expression studies have been done on carotenoid-producing fungi and other organisms. In one study from 2011 (Wozniak et al., 2011), on differential carotenoid production and gene expression in the yeast species *Xanthophyllomyces dendrorhous*, RNA sequencing was used to find genes that are differentially expressed when this yeast was grown in a nonfermentable carbon source. The results from this study suggest that carotenoid production in *X. dendrorhous* is sensitive to environmental factors such as the culture medium, however, they did not look specifically on the effect of calcium.

Another study done on differential gene expression of carotenoid-related genes in *Oncidium* plant cultivars, shows that the upregulation and downregulation of some carotenoid-related genes results in different colorations in the floral tissue of three different Oncidium flowers (Chiou et al., 2010), alteration in color from the Gower Ramsey Oncidium flower have also been altered due to downregulation of different carotenoid genes (Wang et al., 2016).

By lowering the calcium concentration from 2 to 0 mM, Candan and Tarhan (Candan & Tarhan, 2005; Ismaiel et al., 2018) increased the carotenoid and chlorophyll content of *Mentha pulegium*, suggesting calcium may serve as a regulator of carotenoids in plants. However, to our knowledge, there are no studies investigating the effect of calcium on genetic regulation of carotenoid production in *Mucor circinelloides.*

1.1.5 Aim of thesis

The goal of the project is to examine the genomic and molecular basis of calcium influence on carotenoid production in *Mucor circinelloides*. I will investigate how calcium and phosphorus starvation affects gene expression in this species and link this to phenotypic data including pigmentation and carotenoid production.

2 Materials & methods

2.1 Fungal strain

The selection of *Mucor circinelloides* strain was based on the results of the previous study performed by (Dzurendova et al., 2021). The strain was originally obtained in the Food Fungal Culture Collection (FRR; North Ryde, Australia) The stock cultures were stored at -80°C and consisted of asexual fungal spores in a glycerol-NaCl solution. The fungal strain of *Mucor circinelloides* has the collection number FRR5020, and its shortened name is MC2.

2.2 Experimental work

2.2.1 Cultivation of *Mucor circinelloides*

2.2.1.1 Agar plate cultivation

In order to recover fungal culture from the cryo-vials and prepare spore inoculum, cultivation on malt extract agar was done. Malt extract agar (MEA) plates were prepared by dissolving 50 g/L of agar powder (VWR Chemicals - Agar Powder) in deionized water, which was then autoclaved at 115°C for 15 min and subsequently cooled down to 45°C before being poured into Petri dishes (VWR, 9 cm diameter). The MEA Petri dishes were stored at 4°C until use. Before cultivation, the MEA plates were exposed to UV light in a Class 2 biological safety cabinet (Cellegard ES) for 15 min in order to prevent any contamination. Three 5 µL droplets of stock spore suspension (stored in a -80°C freezer) were inoculated onto each MEA plate. The MEA plates were then incubated at 25°C for 4 days in a VWR Inco-line 68 R heat locker. The cultivation on MEA plates was done in four replicates.

2.2.1.2 Cultivation in microtiter plate system

For studying the effect of calcium on pigment production in *Mucor circinelloides*, cultivation of it in the media with different calcium and phosphorus concentrations using a microtiter plate system (Duetz-MTPS) was performed. The microtiter plate system (Duetz-MTPS) consists of deep well 24-square microtiter plates, sandwich covers, and clamp systems to mount microplates on the shaking platform of an incubator. The cultivation in Duetz-MTPS was done using six growth media, each of them contained varying amounts of calcium and phosphorus: P1 is referred to as the reference value of P since the amount has frequently been used to cultivate oleaginous Mucoromycota, P0.5 is half the P1 reference, and P4 is four times the P1 reference.
Stock solutions were prepared and mixed to make the different treatments for *Mucor circinelloides*. In total six treatments, Ca1P1, Ca1P4, Ca1P0.5, Ca0P1, Ca0P4, and Ca0P0.5 were mixed according to the recipe in Table 2.1.

For preparing spore inoculum, *Mucor circinelloides* was cultivated on MEA agar at 25°C for four days. Then 10 mL of sterile saline solution was added to the MEA plates, the spores were harvested by mixing and scraping with single-use plastic loops, and then the spore solution was transferred into Falcon tubes. The obtained spore solution was used as inoculum to inoculate microtiter plates. In each well of the microtiter plates, 7 mL of media (Ca1P1, etc.) was inoculated with 5 µL of spore solution, and a total of 3 wells corresponding to biological replicates per treatment were prepared. Figure 2.1 specifies the experimental design used for each microtiter plate, with only three out of four rows being utilized. Finally, the microtiter plates were mounted on the shaking platform using clamp systems in a shaker (Kuhnershaker X, Climo-shaker ISF1-X) and incubated at 25°C and 250 rpm for 5 days.

Table 2.1 Cultivation media used in the study: *Recipe to stock solutions and treatments.*

100 ml broth:		**Broth parts:**			
Broth part number	***Volume***	***Number***	***Chemical name***	***Extra name***	***Concentration***
1)	60 ml	**1)**	D(+) Glucose Monohydrate	Glucose	88g/600ml
2)	10 ml	**2)**	(NH4)2SO4	Ammonia	1,5g/100ml
3x)	10 ml	**3a)**	MgSO4 7H20 + CaCl2 2H2O	Ca1	1,5g + 0,1g/100ml
4x)	20 ml	**3b)**	MgSO4 7H2O	Ca0	1,5g/100ml
Treatments:					
Ca1P1:	1) + 2) + 3a) + 4a) + Fe + TE	**4a)**	KH2PO4 + Na2HPO4	P1	7g + 2g/200ml
Ca1P4:	1) + 2) + 3a) + 4b) + Fe + TE	**4b)**	KH2PO4 + Na2HPO4	P4	28g + 8g/200ml
Ca1P0.5:	1) + 2) + 3a) + 4c) + Fe + TE	**4c)**	KH2PO4 + Na2HPO4	P0.5	3,5g + 1g/200ml
Ca0P1:	1) + 2) + 3b) + 4a) + Fe + TE	**Fe**	FeCl3 x 6H20	Iron	0,08g/10ml
Ca0P4:	1) + 2) + 3b) + 4b) + Fe + TE	**TE**	ZnSO4 x 7H2O COSO4 x 7H2O CuSO4 x 5H2O MnSO4 x 5H2O	Tracer elements	0,01g 0,001g 0,001g 0,001g/10ml
Ca0P0.5:	1) + 2) + 3b) + 4c) + Fe + TE				

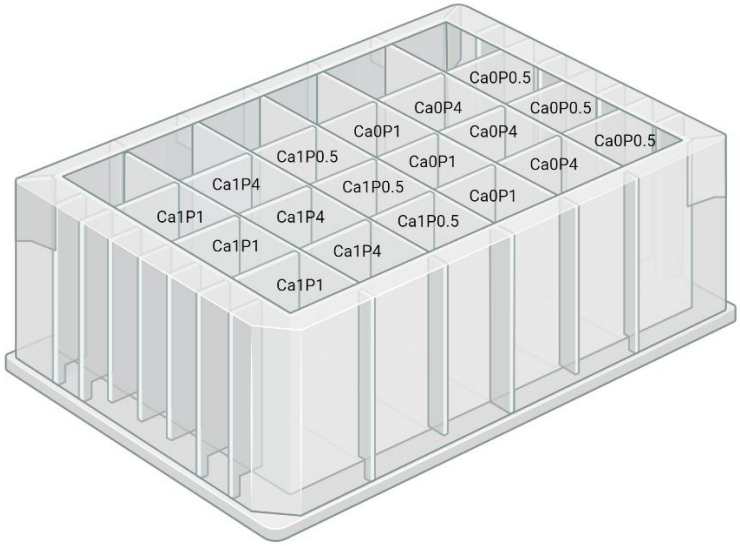

Figure 2.1 Microtiter plate setup for each replicate: *Experimental design in a 24-well microtiter plate.*

2.2.2 Biomass preparation

After the cultivation in Duetz-MTPS, fungal biomass from three identical wells (the same type of media) was merged together and then washed with deionized water using vacuum filtration system. Washed biomass was transferred into sterile Eppendorf tubes (2mL) and immediately placed on dry ice to prevent biomass degradation. This process was repeated for each treatment with a clean vacuum flask and filter. All samples were stored at -80°C until RNA extraction.

2.2.3 RNA extraction

2.2.3.1 RNA extraction

RNeasy Plus Mini kit[1] and the provided by the manufacturer protocol were used to extract RNA from the fungal biomass samples. The "Purification of Total RNA from Animal Tissues" protocol was followed, and prior to RNA extraction, 10 µL Beta-mercaptoethanol was added per 1 mL Buffer RLT. Four volumes of 100% ethanol were added to Buffer RPE before using it for the first time.

Approximately 25 mg of the biomass was weighed and immediately placed in liquid nitrogen. The sample was then grinded to powder with a mortar and pestle. The biomass powder, along with some leftover nitrogen, was transferred to a clean mortar, and 650 uL of Buffer RLT Plus was added after the nitrogen had evaporated. The biomass powder and buffer RLT were homogenized using a clean pestle. The lysate was pipetted into a 2 mL collection tube and centrifuged for 3 min at maximum speed (14,000 rpm).

[1] https://www.qiagen.com/us/products/discovery-and-translational-research/dna-rna-purification/rna-purification/total-rna/rneasy-kits?catno=74104, accessed 12.05.23

The supernatant was carefully removed by pipetting and transferred to a gDNA Eliminator spin column placed in a 2 mL collection tube. The gDNA spin column and collection tube were centrifuged for 30 sec at 10,000 rpm, and the flow-through was saved. In the same volume as the flow-through, 70% ethanol (usually 400-600 µL) was added and mixed well by pipetting.

Next, 650 µL of the sample was transferred to an RNeasy spin column placed in a 2 mL collection tube and centrifuged for 15 sec at 10,000 rpm. The flow-through was discarded by pipetting, and the RNeasy spin column was kept together with the collection tube. Then, 700 µL of Buffer RW1 was added to the spin column, and it was centrifuged for 15 sec at 10,000 rpm to wash the spin column membrane. The flow-through was carefully discarded by removing the RNeasy spin column, and the spin column was transferred to a new 2 mL collection tube. Next, 500 µL of Buffer RPE was added to the RNeasy spin column and centrifuged for 15 sec at 10,000 rpm. The flow-through was again discarded, and the collection tube was reused.

To remove any remaining ethanol residues, 500 µL of Buffer RPE was added to the spin column, which was then centrifuged for 2 min at 10,000 rpm. The RNeasy spin column was then placed into a new 2 mL collection tube and centrifuged for 1 min at 14,000 rpm to ensure that no residues of Buffer RPE were carried over in the collection tube. The spin column was transferred to a 1.5 mL safe cap RNase-free collection tube, and 30 µL of RNase-free water was added directly into the spin column membrane. The lid was closed and centrifuged for 1 min at 10,000 rpm to elute the RNA. Finally, 2.5 µL of the eluted RNA solution was pipetted into a 1 mL tube for quality control shortly after RNA extraction. The safe cap collection tubes were closed and stored at -80°C until sequencing.

2.2.3.2 Quality control

Nanodrop

Using a NanoDrop 8000 microvolume spectrophotometer (Thermo Fisher Scientific, Waltham, Massachusetts, the United States), the purity and concentration of RNA were measured. 1 µL of each sample was pipetted and transferred to the spectrophotometer.

Tapestation

To analyze the quality, quantity, and size of RNA samples, the 4150 TapeStation system (G2992A) with RNA ScreenTape (5067-5576) and RNA ScreenTape Sample Buffer (5067-5577) were used in combination with Agilent Software packages (4150 TapeStation Controller Software and TapeStation Analysis Software). The reagents were first equilibrated at room temperature for 30 min and vortexed before use. The RNA samples were thawed on ice and mixed with 5 µL of RNA sample buffer by adding 1 µL of RNA sample to the buffer. The mixture was vortexed at 2000 rpm for 1 min using an IKA vortexer (MS 3) and then centrifuged (StripSpin I2, Benchmark) for a few seconds. The samples were heated on a PCR machine at 72°C for 3 min and then placed on ice for 2 min. The samples were loaded into the 4150 TapeStation instrument to analyze RNA quality, quantity, and size.

2.2.4 Chemical analyses of fungal biomass

To evaluate the relative content of lipids and carotenoids in the fungal biomass samples, vibrational spectroscopy was applied to the freeze-dried biomass. For estimating relative lipid content Fourier-transform infrared spectroscopy (FTIR) and for estimating relative carotenoid content MultiRAM FT-Raman Spectroscopy (Raman) were used. For a detailed analysis of lipids - total lipid content and fatty acid profile, gas chromatography (GC) was used.

2.2.4.1 Freeze-drying biomass

To freeze-dry the biomass for chemical analysis, the tubes were covered with parafilm, and 3-4 holes were poked in the parafilm. The material was already frozen before going into the freeze-dryer. The tubes were then put into the dryer and maintained at 0.08 bar and -50°C for 2 days for the water to evaporate. The freeze-dried biomass was kept in the freezer at -20°C. To weigh the biomass, the parafilm was removed from the tubes and the dry biomass was weighed using an analytical balance. After weighing, the samples were put in a -20°C freezer.

2.2.4.2 Fourier-transform infrared spectroscopy measurements

Homogenizing

Before FTIR analysis, homogenizing the biomass was done. To homogenize the biomass, a 2 mL screw-cap microcentrifuge tube was filled with 250 mg (710-1180 um diameter) acid-washed glass beads (Sigma Aldrich, USA). A small amount of biomass was then added to the tube, followed by 0.5 mL of distilled water. The tubes were placed in a Precellys Evolution tissue homogenizer (Berlin Instruments, France) at 5500 rpm, 20 sec cycle length, and 6 cycles (2x20 s, 3 runs) to ensure complete homogenization of the biomass.

Plating

Approximately 10 μL of homogenized biomass was pipetted onto an IR transparent 384-well silica microplate, with one free spot between each sample. Three technical replicates were pipetted for each sample. The silica microplate was then dried at room temperature for 30-45 min and then measured in FTIR spectrometer.

Recording FTIR spectra

FTIR spectra were recorded in transmission mode using a high-throughput screening extension (HTS-XT) unit coupled to a Vertex 70 FTIR spectrometer (both Bruker Optik GmbH, Leipzig, Germany). Spectra were recorded in the region between 4000 and 500 cm^{-1}, with a spectral resolution of 6 cm−1, a digital spacing of 1.928 cm−1, and an aperture of 5 mm. For each spectrum, 64 scans were averaged. Spectra were recorded as the ratio of the sample spectrum to the spectrum of the empty IR transparent microplate. In total, 63 biomass spectra were obtained. The OPUS software (Bruker Optik GmbH, Leipzig, Germany) was used for data acquisition and instrument control.

2.2.4.3 MultiRAM FT-Raman Spectroscopy

Determination of the total relative carotenoid content was performed by using a Raman spectrometer. The freeze-dried biomass was transferred into 2 mL screw vials with 400 µL glass inserts until the bottom of the vials was completely covered with biomass, making three technical replicates for each sample. The samples in glass vials were put into a 96-well sample box, for 400 µL flat bottom glass insert and then placed onto a V-grooved sample mount with the samples facing the lens assembly in the MultiRAM FT-Raman spectrometer (Optic GmbH, Germany). The first and the last sample vials contained acetonitrile, used for reference measurements.

2.2.4.4 Gas chromatography-flame ionization detector (GC-FID)

Lipid extraction

BioSpec Norway LIP001 Lipid extraction and GC-FID analysis protocol were used to check the lipid content and fatty acid composition. 20 mg of the freeze-dried biomass together with approximately 250 mg (710-1180 um diameter) of acid-washed glass beads (Sigma Aldrich, USA) were filled in a 2 mL screw-cap polypropylene tube. 500 µL chloroform was added to the mix, and 100 µL of the internal standard was pipetted with a Hamilton syringe. The mix was then homogenized in a Precellys Evolution tissue homogenizer (Berlin Instruments, France) at 5500 rpm, 20 s cycle length, and 6 cycles (2x20 s, 3 runs). The biomass was transferred into glass reaction tubes by washing the polypropylene tube 3 times with 800 µL methanol-chloroform-hydrochloric acid solvent mixture (7.6:1:1v/v). 500 µL of methanol was added into the glass reaction tubes after washing. The mixture was incubated at 90°C for 90 min in a Stuart SBH130D/3 block heater (Cole-Parmer, UK). After the samples were cooled down to room temperature, a small amount of sodium sulphate was added together with 1 mL of distilled water. The sodium sulphate will attract excess water later in the protocol. The mixture was cooled down to room temperature after incubation. To extract the fatty acid methyl esters (FAMEs), 2 mL of hexane was added, and vortex mixed for 10 s before centrifugation at 3000 rpm for 5 minutes at 4°C. The upper organic phase was collected in glass tubes. The upper phase was extracted two more times, in addition, a 2 mL hexane-chloroform mixture (4:1 v/v) was added. To evaporate the solvent, the glass tubes were placed in a Stuart SBH130D/3 block heater (Cole-Parmer, UK) connected to nitrogen at 30°C. The FAMEs were transferred into GC vials by washing the glass tubes 2 times with 750 µL hexane (containing 0,01% butylated hydroxytoluene (BHT, Sigma-Aldrich, USA)), followed by pipette mixing approximately 15 times. The GC vials were stored in a -20°C freezer until GC-FID analysis.

GC-FID analysis

Determination of total lipid content and fatty acid composition was performed by using gas chromatography 7820A System (Agilent Technologies, USA), equipped with an Agilent J&W 121–2323DB-23 column, 20m × 180 μm × 0.20 μm and a flame ionization detector (FID). Helium was used as a carrier gas. The total run time for one sample was 36 min with the following oven temperature increase: initial temperature 70 °C for 2 min, after 8 min to 150 °C with no hold time, 230 °C in 16 min with 5 min hold time, and 245 °C in 1 min with 4 min hold time. The injector temperature was 250 °C and 1 μL of a sample was injected (30:1 split ratio, with split flow 30 mL/min). For the identification and quantification of fatty acids, the Supelco 37 Component FAME Mix (C4–C24 FAME mixture, Sigma-Aldrich, USA) was used as an external standard, in addition to C13:0 TAG internal standard. Measurements were controlled by the AgilentOpenLAB software (Agilent Technologies, USA).

2.2.5 RNA sequencing

RNA sequencing was performed by Novogene Co. to obtain the gene expression profile. Illumina sequencing was ordered with total RNA, 10 million reads per sample, stranded library prep, read length of 150bp and paired-end. Novogene used the RNA-seq technique, where the single-stranded messenger RNAs (mRNAs) are selectively captured or enriched and converted into complementary DNA (cDNA) for library preparation. Novogene also provided quality control of the samples to ensure high-quality sequencing.

2.3 Analyses of spectroscopy and chromatography data

All analyses of FTIR, Raman, and GC-FID data were performed by the Realtek-team with the co-supervisor. Boxplots were made to visualize the data.

2.4 Analyses of gene expression data

2.4.1 Preprocessing of gene expression data

The nf-core/RNAseq pipeline[2] was used to process and analyze the raw RNA sequencing data. The pipeline is built using Nextflow, which is a workflow tool that runs tasks across multiple computing infrastructures. In this analysis, nf-core/RNAseq version 3.8 were used together with Nexflow on NMBUs high-performance computing resource; Orion[3]. Nextflow was installed using the Orion singularity container.

As input, nf-core/RNAseq needs RNA sequencing data, a reference genome and annotation. The sample sheet input is a comma-separated file with 4 columns and a header row, and contains sample name, the fastq file paths, and the strandedness of the samples (reverse strandedness in this case). Samplesheet path was added to the '--input' parameter.

[2] https://nf-co.re/rnaseq, accessed 12.05.23
[3] https://orion.nmbu.no/, accessed 12.05.23

The reference genome assembly and annotation were made by Tu-Hien To, as part of the Earth BioGenome Project Norway. Tissue from the same individual/clone was used for whole-genome sequencing as in this experiment. The genome assembly was done by first removing short reads (<4000bp) and low-quality ones (q<7), then assembled with Flye version 2.9.1 (Kolmogorov et al., 2019). The assembly were then evaluated with Inspector version v1.0.2 (Chen et al., 2021) and Merqury version v1.3 (Rhie et al., 2020) for accessing the quality (QV) and completeness; and with Busco version 5.4.3 (Manni et al., 2021) for accessing the quantity of conserved genes. Annotation was done with the funannotate pipeline version v.1.8.13[4], using the RNA-seq data generated in this project. This pipeline was developed to annotate fungi and is widely used. RNA-seq samples were merged to the corresponding strain to serve as evidence for the annotation. The assemblies were first cleaned to remove the repetitive contigs, then masked the repeat regions using the default masker tantan in funannotate. The gene models were predicted with several methods and then combined into one by Evidence Modeler. Functional annotation was run with all the implemented tools in the pipeline: Pfam, InterProScan, Eggnog, UniProtKb, Pobius, antiSMASH, MEROPS. The reference genome filepath was added to the parameter '-- fasta', and the annotation file path to the '--gff' parameter in the Nextflow RNAseq script.

Nf-core/RNAseq starts with pre-processing of the RNA sequencing data, followed by genome alignment and quantification. After this nf-core/RNAseq does some post-processing and provides a multiQC report. To align nf-core/RNAseq uses STAR as a default. STAR is used to map the raw FastQ reads to the reference genome. STAR is a fast universal RNA-seq aligner, which has a good accuracy. The STAR algorithm consists of two major steps, which are seed searching and clustering (Dobin et al., 2013).

To perform the quantification nf-core/RNAseq use Salmon as a default. Salmon is a fast transcript quantification tool (Patro et al., 2017). It requires a set of reference transcripts and a set of Fastq files containing reads to quantify. Salmon runs two different modes, the first requires a built index for the transcriptome, and then can process reads directly. The second mode requires only a provided FASTA file of the transcriptome and a sam or bam file containing alignments. By default, nf-core/RNAseq uses the genome fasta and gtf file to generate transcript FASTA files and build the Salmon index (Salmon mode 1).

Nf-core/RNAseq was used with default settings. Since *Mucor circinelloides* is not a part of the iGenomes reference, '--fasta' was added to have the path to the FASTA genome file, and '--gff' was added to have the path to the GFF3 annotation file.

Nextflow gives a list of different output files, including an HTML report that visualizes a summary of all samples. The results in the multiQC HTML report collate QC from FastQC, Cutadapt, SortMeRNA, STAR, RSEM, HISAT2, Salmon, SAMtools, Picard, RSeQC, Qualimap, Preseq and featureCounts. Nextflow also gives a list of output files to do more analysis on, of these, a gene count tsv file both scaled and not scaled is represented.

[4] https://github.com/nextgenusfs/funannotate, accessed 12.05.23

2.4.2 Differential gene expression analyses

The salmon.merged.gene_counts_scaled.tsv from Nextflow output and the sample information metadata file were imported into R for further data analysis using the R package *utils* and reformatted to be used in differential gene expression analysis.
The metadata file was made with information about calcium content, phosphorus amount, name from Novogene, the full name of the samples, replicate number and group which is the common name with information about both calcium content and phosphorus level.
To identify differentially expressed genes (DEGs) between the different conditions, the *DESeq2* package in Rstudio was used. DESeq2 evaluates the quantitative differences between contrasting groups in the dataset (Love et al., 2014). To start the differential gene expression analysis a DESeq2 dataset matrix was made using the processed count data table and the sample information table. The design of the statistical test was comparing samples by groups. To clean up the data, all rows with rowsum = zero were removed from the dataset. This was done using the rowSums() function from the *BiocGenerics* package. The actual differential gene expression analysis was done by running the DESeq() function with the data matrix as input with default settings.
The package DESeq2 provides methods to test for differential expression by use of negative binomial generalized linear models. The estimates of dispersion and logarithmic fold changes incorporate data-driven prior distributions (Love et al., 2014). Because of the binominal model, only two and two comparisons can be done. Models including all treatments are more parametrized and more difficult to interpret. Since we are mostly interested in the effect of calcium in the presence of low phosphate, the comparison between Ca0P0.5 and Ca1P0.5 was used as the contrast for the negative binomial generalized linear model. The interest for the effect of calcium in the presence of low phosphate comes from the study done by Dzurendova et. al. and visual laboratory results prior to genomic analysis. Further analysis focused on this comparison, however we manually looked at expression levels across all treatments for our top candidate genes (see further down).

To visualize the DESeq data PCA plots were made using ggplot() from the *ggplot2* package. Two PCA plots were made, one with PC1 on the x-axis and PC2 on the y-axis and the second one with PC1 on the x-axis and PC4 on the y-axis. The color of the dots in the plots is representing the samples and which group they belong to.
A volcano plot was made to visualize DEGs in the contrast (Ca0P0.5 vs. Ca1P0.5). This was done using the plot function, with log2FoldChange on the x-axis and -log10(padj) on the y-axis. The selection of upregulated DEGs was set to padjust values under 0.05 and log2Foldchange over 2. The selection of downregulated DEGs was set to padjust value under 0.05 and log2FoldChange under -2. To highlight genes that are of special interest, padjust values under 0.00005 and log2FoldChange over 4 were selected for upregulated DEGs, padjust values under 0.005 and log2FoldChange under -4 were selected for downregulated DEGs.
To visualize the gene expression in the top DEGs as well as candidate genes from the literature, boxplots were made using the ggplot() function.

2.4.3 Gene Ontology enrichment

To investigate the functional significance of the top down- and upregulated genes, gene ontology (GO) enrichment analyses implemented in the tool Gprofiler; GO enrichment tool[5] were used. The process of enriching GO terms involves analyzing groups of genes and utilizing the Gene Ontology classification system, which categorizes genes into predefined groups based on their functional attributes.
Gprofiler is a public web server for characterizing and manipulating gene lists. Although there is no general rule, GO enrichment analysis usually gives more meaningful results with more genes than the top candidates selected in the step above. For these analyses less conservative cut-off values were selected for identifying top DEGs, with an upper limit padj < 0.05 and the log2FoldChange value over 0 for upregulated DEGs and a log2FoldChange value under 0 for dowregulated DEGs.

Since the *Mucor circinelloides* genome was not annotated by ENSEMBL the gene names are not recognized by Gprofiler. To alleviate this, we identified ortholog genes from the latest ENSEMBL version of baker's yeast (*Saccharomyces cerevisiae*, V. R64-1-1,[6]) using orthofinder (V.2.5.4, (Emms & Kelly, 2019). The yeast orthologs corresponding to top DEGs in *Mucor circinelloides* were then imported into Gprofiler.

The gene list with up- and downregulated genes with the information on yeast genes were put into the g:Convert gene identifier convention tool in the web server. *Saccharomyces cerevisiae* were set as the organism, and the target namespace was set as GO. The gene list was put in the query space and run with the options. Then looking into the g:GOSt tool, a statistical enrichment analysis of the gene list was made with the same options as in g:Convert. g:GOSt performs functional profiling of the gene list using various kinds of biological evidence. The tool performs statistical enrichment analysis to find the over-represented gene ontology term and biological pathways. The option 'Highlight driver terms in GO' were ticked off, but no further advanced options were used in the analysis.

2.4.4 Analyses of candidate genes and Top DEGs

In addition to GO enrichment, the functional significance of a handful of top DEGs were analyzed manually in more detail. Additionally, candidate genes from the literature were investigated. Orthologs to candidate genes were identified using BLAST, using both the web tool (V.2.13.0, (Altschul et al., 1990)) as well as the command-line tool that can be used on a high-performance computing resource. BLAST stands for "Basic Local Alignment Search Tool" and it's task is to find regions of similarity between biological sequences. When searching in the protein database, BLASTp was used (default settings). Additionally, we used BLAST to functionally annotate top DEGs which lack functional annotation from the automated annotation described above. For top hits, alignments were manually inspected to ensure the identification of likely orthologs.

[5] https://biit.cs.ut.ee/gprofiler/gost, accessed 12.05.23
[6] https://www.ensembl.org/Saccharomyces_cerevisiae/Info/Index?db=core, accessed 12.05.23

3 Results

3.1 Visual inspection of the fungal biomass

Biomass pigmentation varied significantly between treatments, with some variation between biological replicates (Figures 3.1 to 3.3). Samples from the biological replicate 1 (Figure 3.1) are mostly milky yellow, but a visibly higher content of carotenoids is observed in biomass grown in calcium-lacking media with low phosphorus (Ca0P0.5). Samples from the biological replicate 3 (Figure 3.2) also have a milky yellow tone on all samples, except the sample Ca0P0.5, that have a visibly higher content of carotenoids. Ca0P0.5 from replicate 3 does not have as much of a difference in pigmentation as the one in the biological replicate 1. The samples with the least content of carotenoids are Ca1P0.5, in both biological replicates 1 and 3. Figure 3.3 shows the difference in carotenoid content between Ca1P0.5 and Ca0P0.5 and the variability between individual biological replicates of Ca0P0.5.

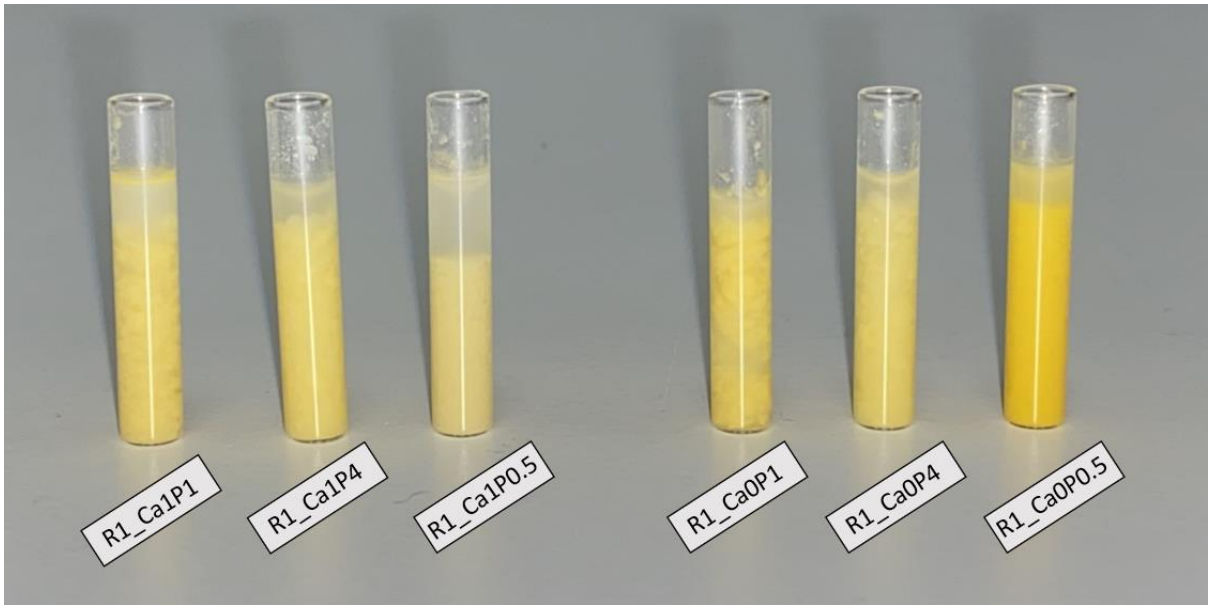

Figure 3.1 Biomass from the biological replicate 1 in glass vials mixed with water: *Biomass from all samples in replicate 1.*

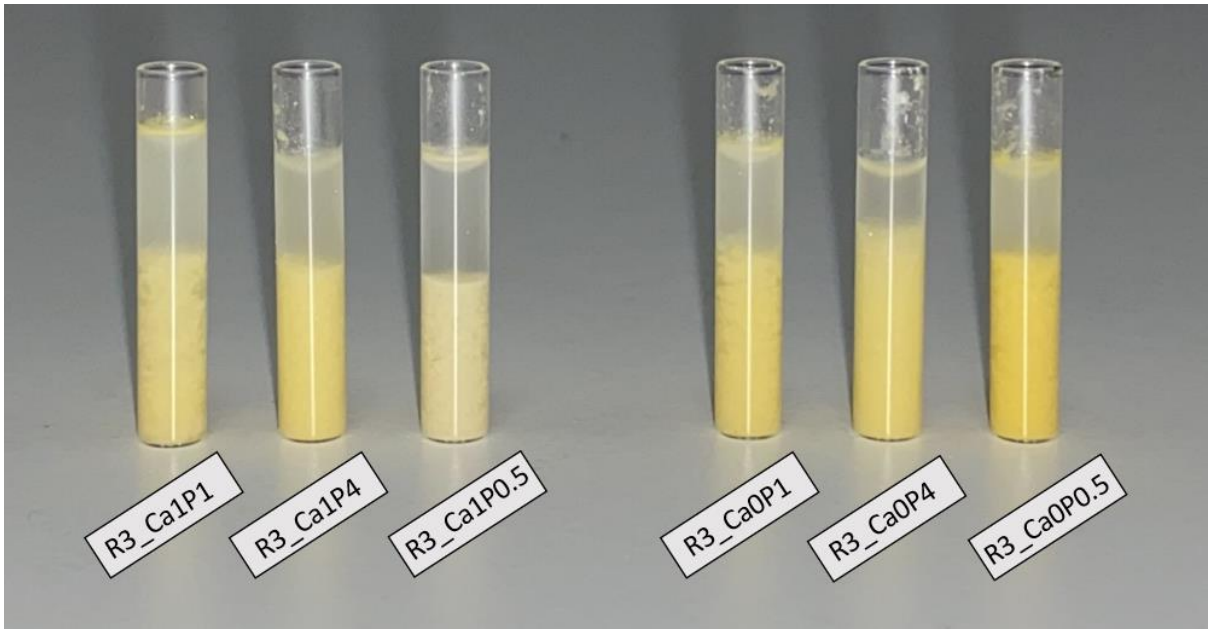

Figure 3.2 Biomass from the biological replicate 3 in glass vials mixed with water: *Biomass from all samples in replicate 3.*

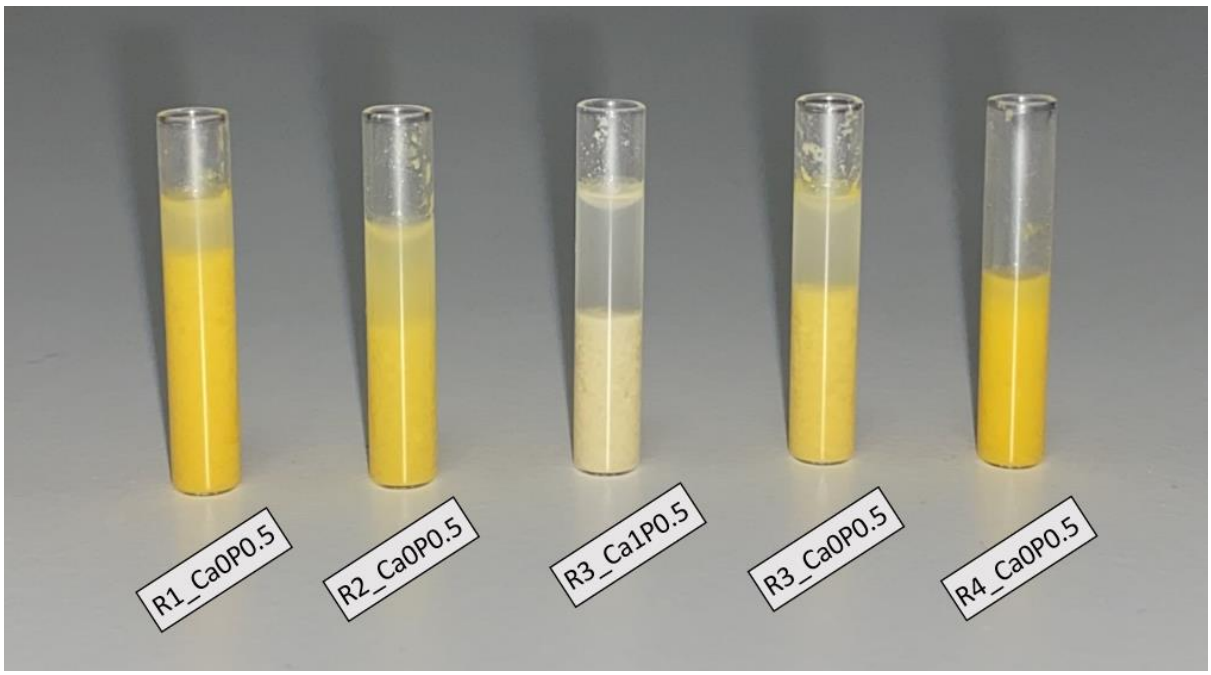

Figure 3.3 Biomass from the biological replicates 1, 2, 3 and 4 in glass vials mixed with water: *Biomass from Ca0P0.5 from replicate 1, 2, 3 and 4, and biomass from Ca1P0.5 from replicate 3.*

3.2 Chemical analyses of the fungal biomass

3.2.1 Total lipid content and fatty acid profile by GC-FID

The mean of the total lipid content ranges from 30 - 50%, with some variance differences between treatments (Figure 3.4). In each phosphorus group, the lipid content is almost the same across the two calcium levels. Between the phosphorus levels, there are some slight differences, with P4 having the least percentage of lipids (32%), P1 having the highest percentage (48%) of lipids, and P0.5 in the middle (40-42%). P4 has the highest standard deviation within each group.

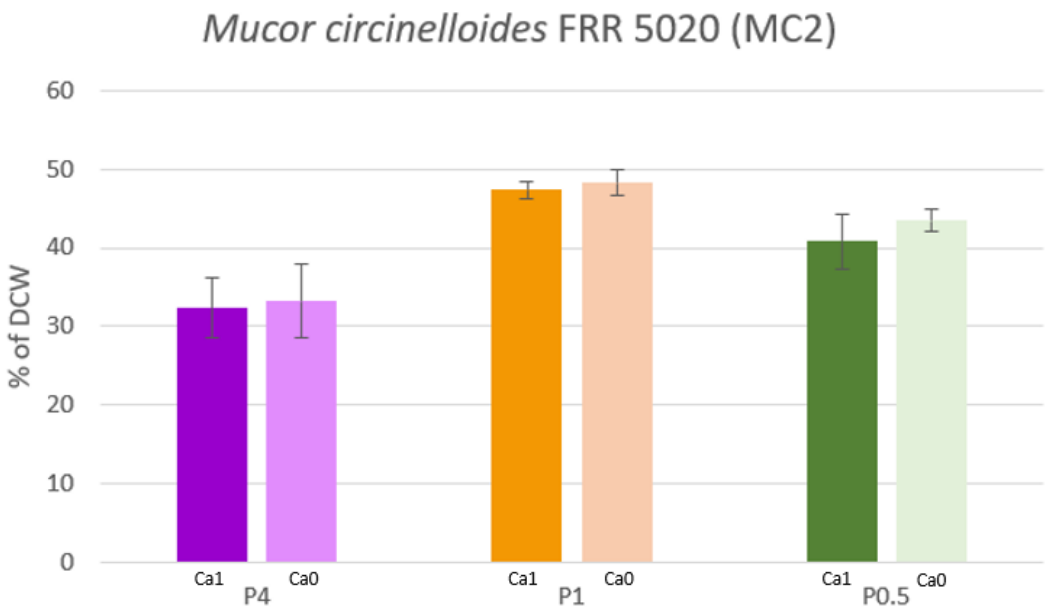

Figure 3.4 Mean percentage of total lipid content in all samples: *Lipid percentage of biomass in all samples grouped by calcium(present(1)/absent(0)) Samples colored by group; Ca0 = light color, Ca1 = dark color, P05 = green, P1 = orange, P4 = purple.*

The lipid profile from each sample was measured by the GC-FID. The lipid profile was very similar for all sample groups, with minor differences in the amount of the different fatty acids (Figure 3.5). The predominant fatty acid was oleic acid (C18:1n9c), the second most predominant was palmitic (hexadecanoic) acid (C16:0), and the third was Gamma-linoleic acid (C18:3n6), which is an essential fatty acid. Linoleic acid (C18:2n6c) and stearic octadecanoic acid (C18:0) have almost the same amount, being the fourth most dominant fatty acids. The minor fatty acids were Palmitoleic acid (C16:1), (C14:0), Nervonic acid (C24:1n9), (C20:0), (C18:2n6t), (C17:0) and (C12:0).

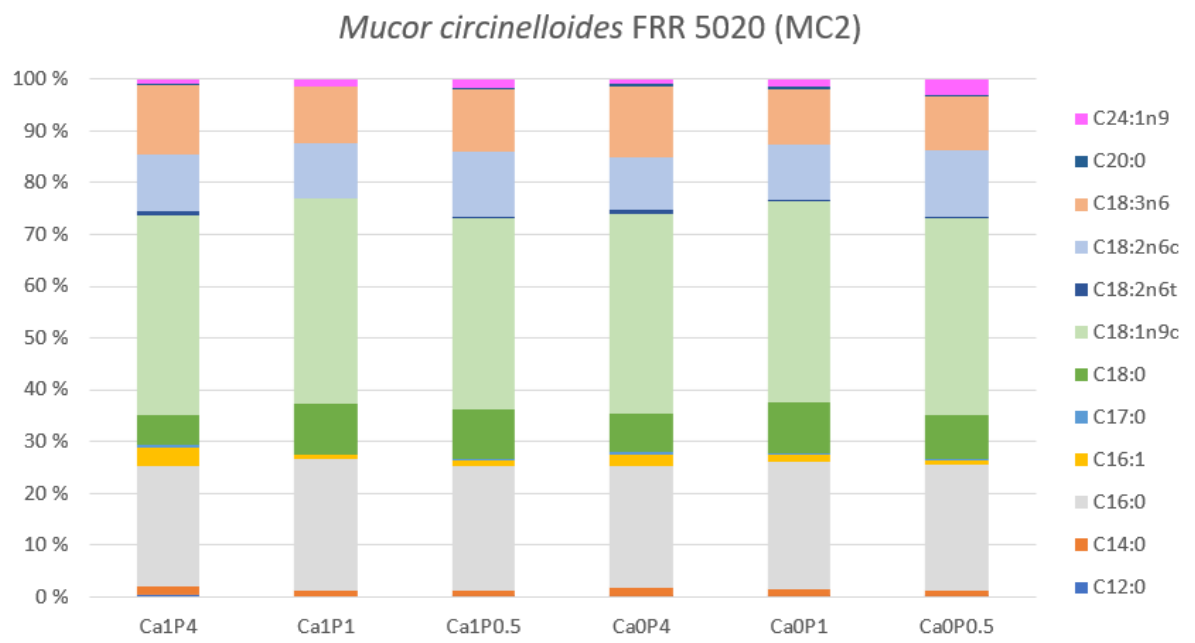

Figure 3.5 Fatty acid profile for all samples: *Lipid profile presenting fatty acids found in all samples grouped by calcium (present (1)/absent (0)) and phosphorus (0.5/1/4).*

3.2.3 Relative carotenoid content by Raman spectroscopy

Carotenoid content in Ca0P0.5 was significantly higher than for all other treatments, with a mean value of *RI_1523/RI_1445* of 0,5 (Figure 3.6). Carotenoid content for both P1 and P4 samples was around 0,38, with a slight increase in carotenoids when calcium was absent (Ca0). There are no huge standard deviations across replicates in these treatments. The standard deviation for Ca0P0.5 was higher than for the other treatments, meaning there is a difference between replicates for this treatment, however, the carotenoid content is still consistently higher than for other treatments.

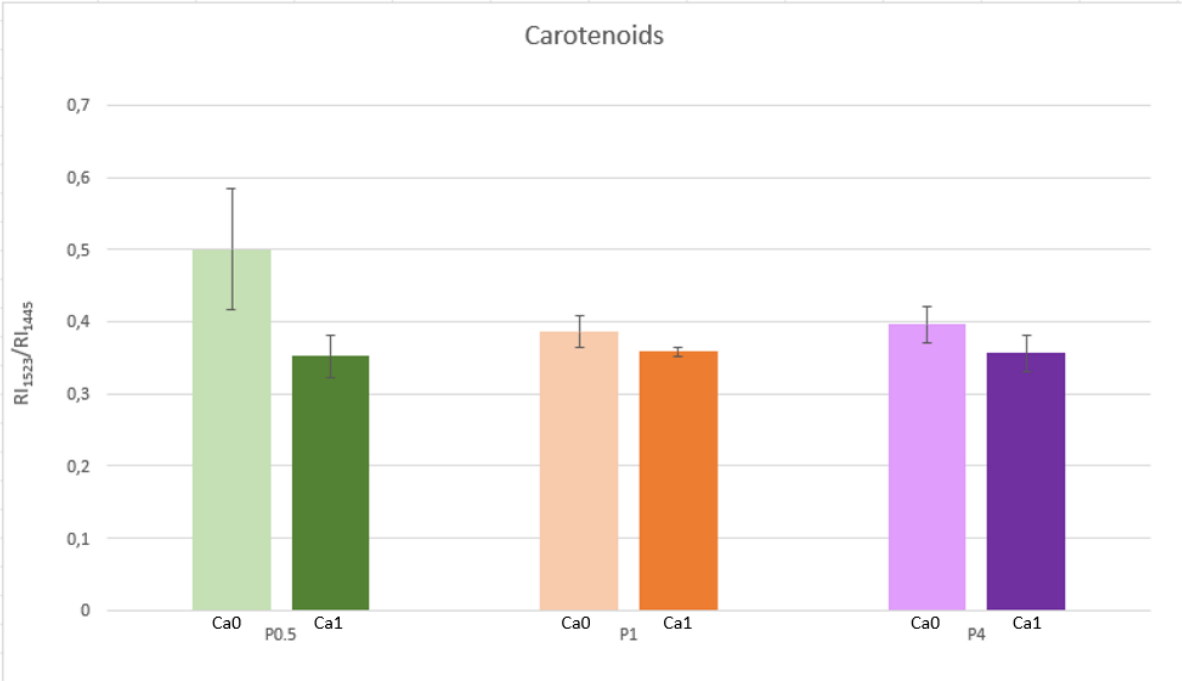

Figure 3,6 Mean relative carotenoid content for all samples: *Carotenoid content measured in the mean value of RI_1523/RI_1445. Samples colored by group; Ca0 = light color, Ca1 = dark color, P05 = green, P1 = orange, P4 = purple.*

The high difference in carotenoid content is clearly visible between Ca0P0.5 and Ca1P0.5 on Figure 3.3, and the spectroscopic data that confirms this difference (Figure 3.6).

3.3 RNA Quality and Concentration

RNA quality and concentration were measured before sending the samples for sequencing, using Nanodrop and Tapestation. The quality and concentration were also measured by Novogene right before sequencing. In Table 3.1, both ng/µL and RIN values are listed for each sample. Nanodrop measured RNA concentration, and it was generally very high, except for a few samples (MC2_R2_Ca1_P4, MC2_R2_Ca1_P0.5, MC2_R2_Ca0_P4, MC2_R4_Ca1_P4). RNA concentration measured by Tapestation was lower than the concentration measured by nanodrop, that was 50% or less. RNA concentration measured by Novogene was even lower than Tapestation measurements, except for three measurements where Novogene was higher than Tapestation (MC2_R1_Ca0_P0.5, MC2_R2_Ca0_P0.5, MC2_R4_Ca0_P4). RIN RNA quality measurements from Tapestation and Novogene were high, with the lowest value of 6.6 from Tapestation. Three of the samples were not sequenced, because of their low concentration (MC2_R2_Ca1_P4, MC2_R2_Ca1_P0.5, MC2_R4_Ca1_P4).

Table 3.1 Concentration and quality of RNA samples: *Concentration of RNA measured in ng/µL from Nanodrop, Novogene and Tapestation. Quality of RNA samples measured in RIN values from Tapestation and Novogene. Samples not sequenced are marked with a (*).*

Sample	Nanodrop ng/µl	Novogene ng/µl	Tapestation ng/µl	Tapestation RIN	Novogene RIN
MC2_R1_Ca1_P1	191,5	16,96	88,2	10	9,8
MC2_R1_Ca1_P4	88,78	12,76	30,3	9,7	10
MC2_R1_Ca1_P0.5	465,4	41,18	43,6	6,6	8,7
MC2_R1_Ca0_P1	291,5	27,62	43,6	9,5	9,6
MC2_R1_Ca0_P4	221,5	22,32	38,5	10	10
MC2_R1_Ca0_P0.5	587,3	126,15	44,0	9,7	10
MC2_R2_Ca1_P1	180,8	8,76	50,5	10	10
MC2_R2_Ca1_P4*	71,83	2,71	41,7	10	10
MC2_R2_Ca1_P0.5*	35,84	2,53	19,3	9,1	8,8
MC2_R2_Ca0_P1	435,6	16,45	131	10	10
MC2_R2_Ca0_P4	42,41	6,91	14,1	9,8	10
MC2_R2_Ca0_P0.5	375,6	81,84	44,0	9,4	9,1
MC2_R3_Ca1_P1	195,7	16,71	85,8	9,0	7,8
MC2_R3_Ca1_P4	106,4	6,86	40,4	9,8	9,9
MC2_R3_Ca1_P0.5	243,1	12,24	43,7	9,1	7,3
MC2_R3_Ca0_P1	174,9	10,45	47,1	9,8	9,7
MC2_R3_Ca0_P4	196,2	12,47	52,2	10	10
MC2_R3_Ca0_P0.5	255,7	14,83	121	10	7,9
MC2_R4_Ca1_P1	358,5	13,7	78,4	9,9	10
MC2_R4_Ca1_P4*	43,29	1,99	15,8	9,9	10
MC2_R4_Ca1_P0.5	108,3	9,25	36,8	9,3	8,8
MC2_R4_Ca0_P1	268,6	13,04	97,2	10	10

3.4 Gene expression data quality control

Mapping reads to the reference genome was done using STAR, with a mean number of 14 million reads mapped (Figure 3.7). Most of the reads map uniquely. The sample with the most mapped reads is MC2R4_1(R4_Ca1P1), with 21 million reads. The sample with the least mapped reads is MC2R2_4 (R2_Ca0P1), with 12 million reads. All samples had some reads mapped to ‘many loci’ and mapped to ‘too many loci’. Just a small number of reads were not mapped. Furthermore, all samples had high base call accuracy with an average Phred score > 30 (Figure 3.8).

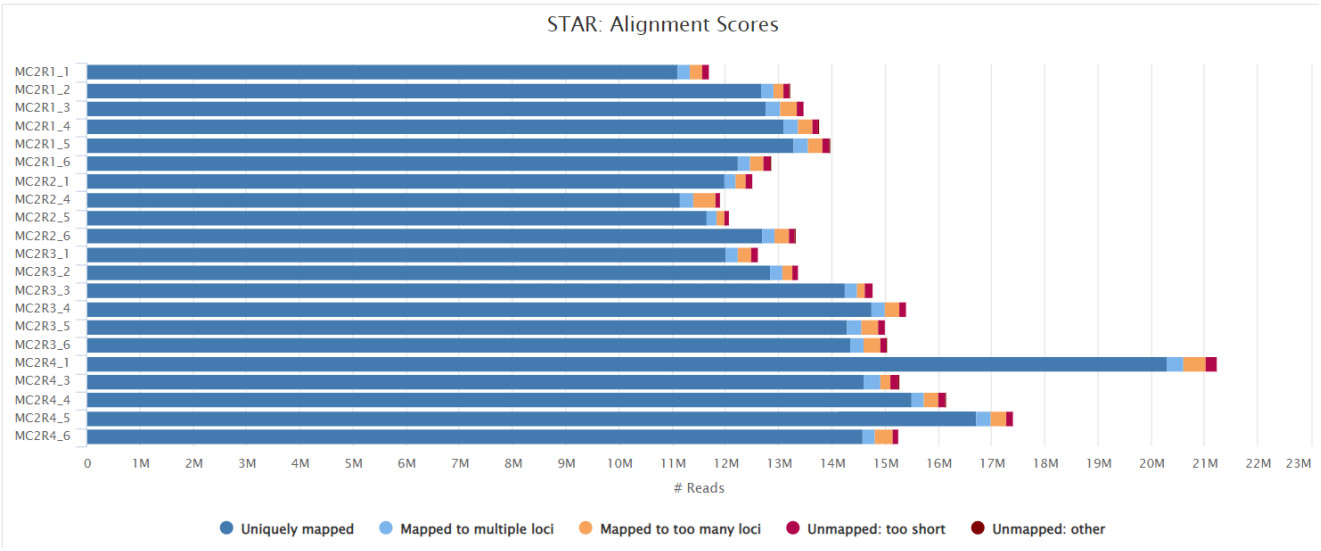

Figure 3.7 Alignment scores measured in the number of mapped reads: *Number of mapped reads in millions from the 21 samples that were sequenced. The figure was generated using Nextflow.*

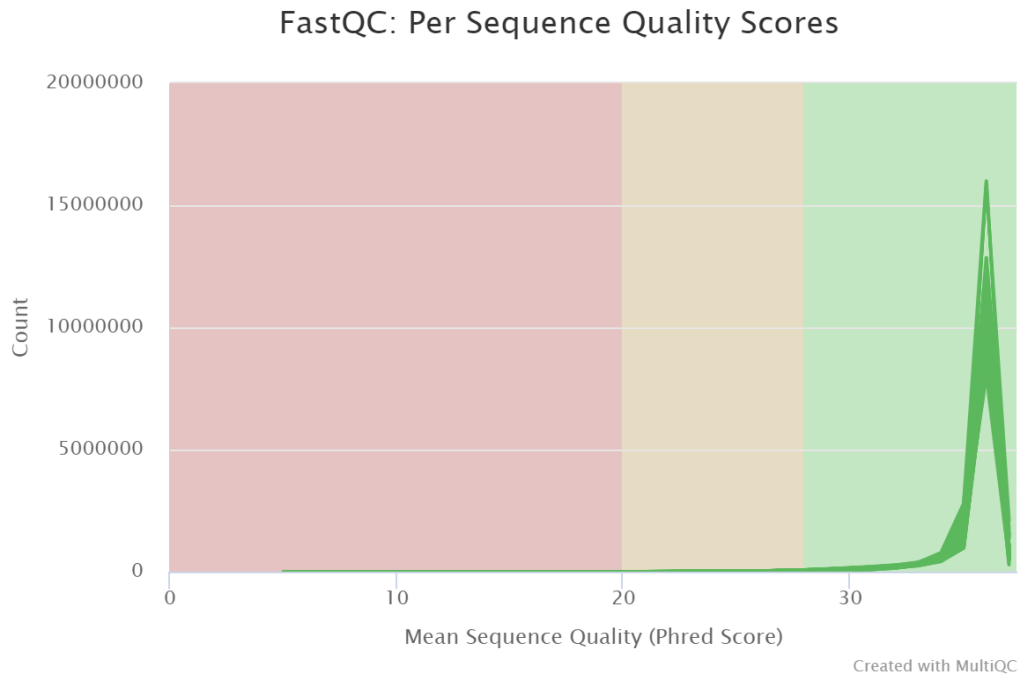

Figure 3.8 Plot of per sequence quality scores of all sequenced samples: *Per sequence quality scores created with MultiQC. One graph line for all fastq files that were run through FastQC. Mean sequence score on the x-axis and the number of sequences with that score on the y-axis. Green lines indicate high quality. The figure was generated using Nextflow.*

3.5 Principal component analysis

To visualize the clustering of raw sequencing data across treatments and replicates principal component analysis (PCA) was done on all sequenced samples (Figure 3.9). On the PC1 and PC2 analysis, samples cluster according to phosphorus amount. Especially the samples with the highest amount of phosphorus (P4, purple) clusters far away from the others. Most of the samples with phosphorus level 1 (orange) cluster together, but two samples are outliers from Ca0. Samples from phosphorus level 0.5 (green) cluster in two groups based on calcium level, but with one outlier from Ca1 that clusters together with Ca0. The PC1 axis explains 34,2% of the variance and the PC2 axis explains 24% of the variance.
In the PC1 and PC4 plot, one can see that PC4 separates calcium treatments, and where Ca1P0.5 clusters together. The two outliers from Ca0P1 (light orange) are still away from each other but with a lower percentage on the y-axis (PC4). The PC1 axis explains 34,2% variance and the PC4 axis explains 6,3% variance.

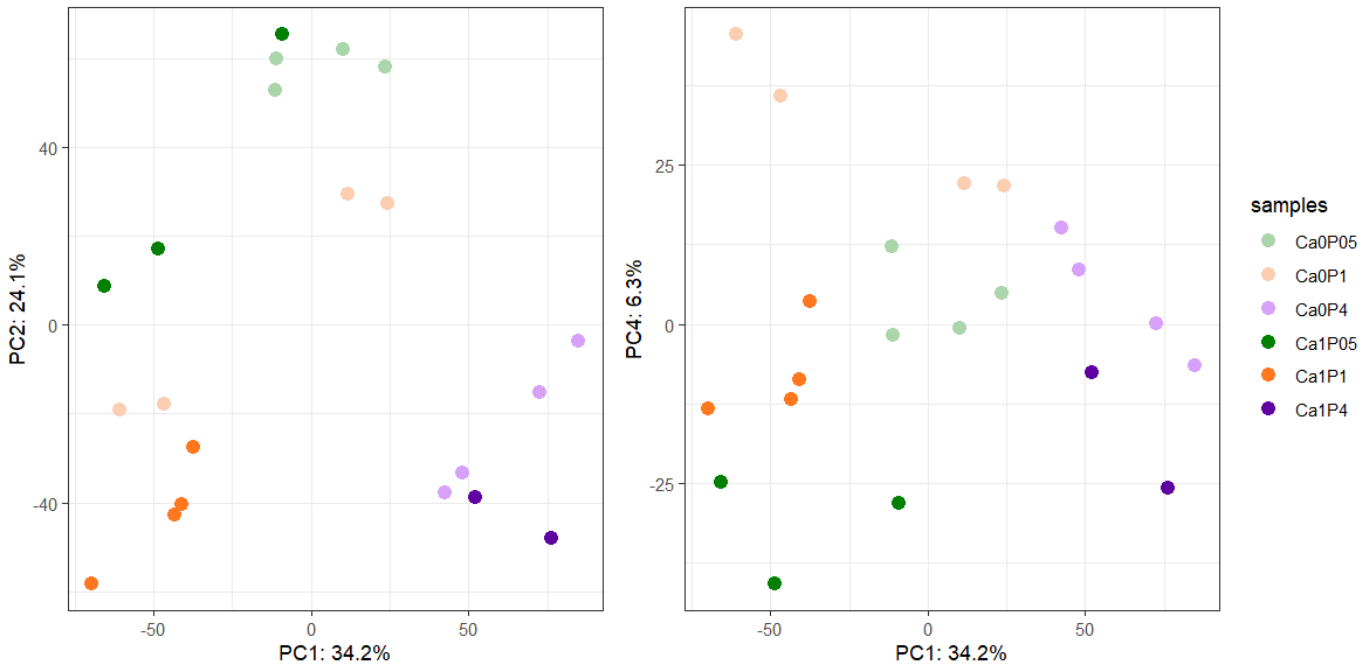

Figure 3.9 Principal component analysis plot on all sequenced samples: *Samples plotted along the PC1 and PC2 axis, and the PC1 and PC4 axis. Samples are colored by treatment according to legend.*

3.6 Upregulated and downregulated differentially expressed genes

By comparing expression levels between Ca0P05 and Ca1P05, a total number of 2556 DEGs were identified (Figure 3.10). To isolate biologically and statistically significant DEGs, a cutoff of padj under 0.05 and log2FC values over and under 2 or -2, respectively, yielding 276 significantly upregulated DEGs and 211 significantly downregulated DEGs (Figure 3.10).

The upregulated DEGs vary more in p-adjust value and log2FoldChange than downregulated DEGs. The lowest p-adjust value is $2.799772e^{-40}$ and the highest log2FoldChange is 21,3. Using more stringent filtering criteria (p-adjust value under 0.00005 or under 0.005 & log2FoldChange over or under 4 for upregulated and downregulated DEGs, respectively), we selected the most extreme DEGs for more in-depth analyses, as they are likely to influence the phenotypic variation in carotenoid production. This yielded 24 upregulated DEGs and 14 downregulated DEGs (Figure 3.10).

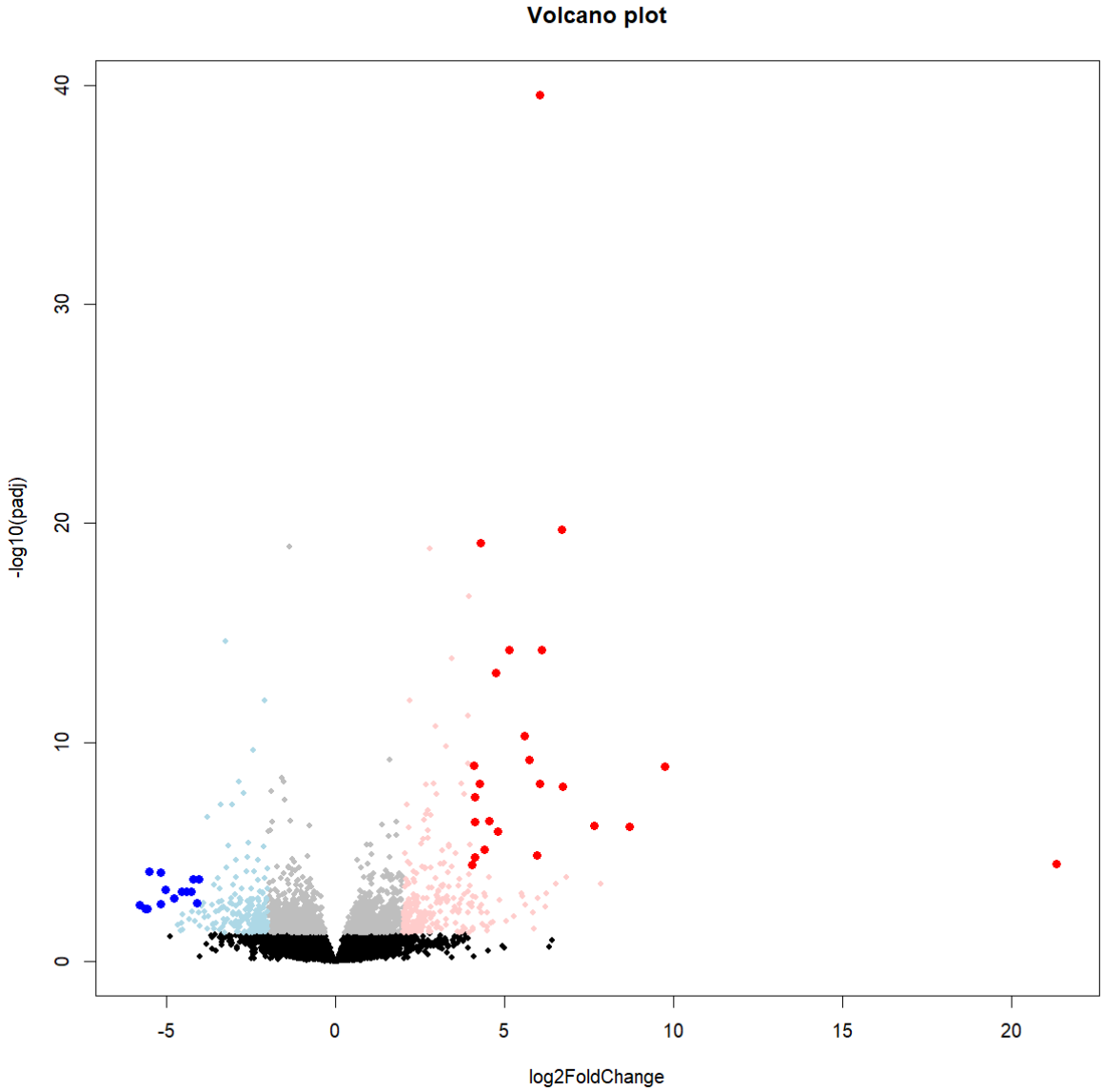

Figure 3.10 Volcano plot on up- and downregulated DEGs on contrast (Ca0P05, Ca1P05): *Upregulated DEGs with a p-adjust value under 0.05 & log2FoldChange over 2 are colored in light red. Upregulated genes with a p-adjust value under 0.00005 & log2FoldChange over 4 are colored in dark red. Downregulated genes with a p-adjust value under 0.05 & log2FoldChange under -2 are colored in light blue. Downregulated genes with a p-adjust value under 0.005 & log2FoldChange under -4 are colored in dark blue.*

In figure 3.11, total genes vs. gene orthologs from yeast are plotted in a barplot. The total genes with a nonzero total read count are 11458, of these 5159 have orthologs found in yeast. Approximately 50% of the genes have no further information that can be used in GO enrichment, meaning a lot of lost information. This is also the trend for both upregulated and downregulated genes as well. Only 50% of the up- and downregulated genes have yeast orthologs. In figure 3.11, the same cut-off as the GO enrichment analysis is used for the up- and downregulated genes.

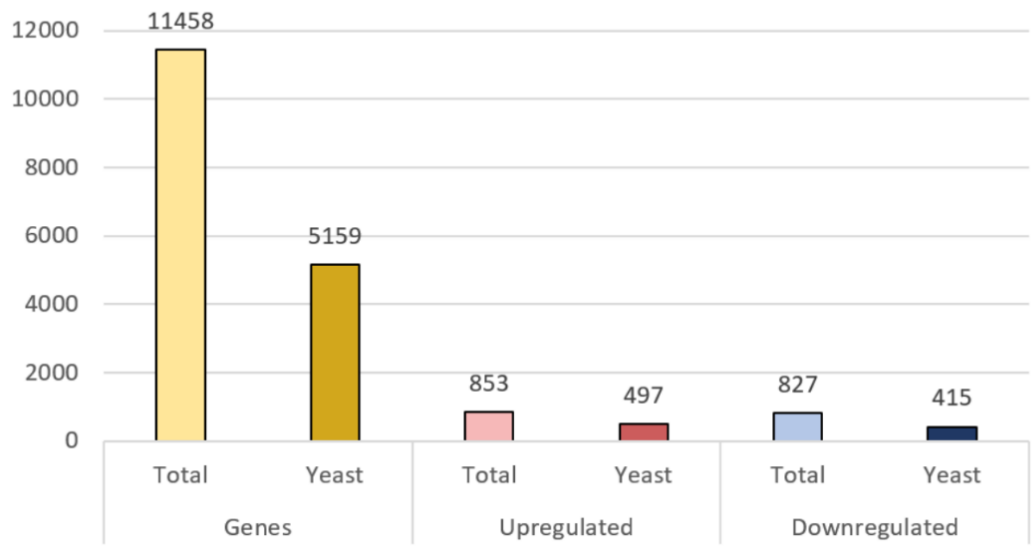

Figure 3.11 Expressed yeast orthologs found in Mucor circinelloides *Number of genes with nonzero total read count for the total dataset (light yellow) and genes with identified yeast orthologs, as well as total downregulated DEGs (light red), downregulated DEGs with yeast orthologs (dark red), total upregulated DEGs (light blue), and upregulated DEGs with yeast orthologs (dark blue) and the number of ortholog genes found in yeast.* ***DEGs are from the contrast*** *(Ca0P05, Ca1P05).*

3.7 Gene ontology enrichment analyses

Gene ontology (GO) enrichment analyses was done using Gprofiler to evaluate the function of the top DEGs. The detailed results, including molecular function, biological process, and cell components from Gprofiler are presented in figures 3.12 to 3.17. Gprofiler also provides GO context maps over all the terms, to see the different terms being connected. These maps can be accessed through inserting terms from appendix 1 for the upregulated genes, and appendix 2 for the downregulated genes into g:Profiler.
The three first figures are the enrichment of the 497 DEGs with yeast orthologs (Figures 3.12 to 3.14). The three last figures are the enrichment of the 415 DEGs with yeast orthologs (Figures 3.15 to 3.17).

3.7.1 Function of the upregulated DEGs

The molecular function of the upregulated DEGs are presented in figure 3.12. The driver terms in the molecular function are "*structural constituent of ribosome*", "*RNA binding*", "*transporter activity*", "*oxidoreductase activity*", "*ion binding*", "*phosphotransferase activity, alcohol group as acceptor*", "*quatemary ammonium group transmembrane transporter activity*", "*L-isoleucine transmembrane transporter activity*" and "*L-glutamine transmembrane transporter activity*". The driver terms are usually a broad and general term, built on smaller terms, which in turn are connected to each other.
Several of the molecular function terms are transmembrane transporter terms, indicating this being a general and over-represented term group. The general "*binding*" term includes a few more specific terms, like "r*RNA binding*" and "*ion binding*".

GO:MF

stats

Term name	Term ID	p_{adj}	$-\log_{10}(p_{adj})$
structural constituent of ribosome	GO:0003735	1.763×10^{-35}	
structural molecule activity	GO:0005198	9.703×10^{-20}	
RNA binding	GO:0003723	1.092×10^{-6}	
organic cyclic compound binding	GO:0097159	4.127×10^{-5}	
heterocyclic compound binding	GO:1901363	7.458×10^{-5}	
transporter activity	GO:0005215	7.968×10^{-5}	
transmembrane transporter activity	GO:0022857	8.413×10^{-5}	
binding	GO:0005488	1.056×10^{-4}	
rRNA binding	GO:0019843	4.407×10^{-4}	
oxidoreductase activity	GO:0016491	1.445×10^{-3}	
ion binding	GO:0043167	4.488×10^{-3}	
salt transmembrane transporter activity	GO:1901702	1.215×10^{-2}	
nucleic acid binding	GO:0003676	1.243×10^{-2}	
phosphotransferase activity, alcohol group as acceptor	GO:0016773	1.282×10^{-2}	
oxidoreductase activity, acting on NAD(P)H, quinone o...	GO:0016655	1.628×10^{-2}	
oxidoreductase activity, acting on NAD(P)H	GO:0016651	2.800×10^{-2}	
organic anion transmembrane transporter activity	GO:0008514	3.653×10^{-2}	
quaternary ammonium group transmembrane transpo...	GO:0015651	5.000×10^{-2}	
L-isoleucine transmembrane transporter activity	GO:0015188	5.000×10^{-2}	
branched-chain amino acid transmembrane transporte...	GO:0015658	5.000×10^{-2}	
L-glutamine transmembrane transporter activity	GO:0015186	5.000×10^{-2}	

Figure 3.12 Upregulated DEGs molecular function: *The molecular functions of the upregulated differentially expressed genes from contrast (Ca0P05, Ca1P05) used as input in Gprofiler. 497 gene orthologs to yeast are used as input queries. Highlighted terms are driver terms in each component.*

The biological process of the upregulated differentially expressed genes are presented in Figure 3.13. The driver terms in the biological process are "*cytoplasmic translation*", "*ribosome biogenesis*", "*localization*", "*response to chemical*", "*amide transport*", "*positive regulation of catalytic activity*", "*regulation of Rho protein signal transduction*", "*apoptotic process*", "*negative regulation of intracellular signal transduction*" and "*dephosphorylation*". The general "*cellular process*" and "*metabolic process*" both include more specific terms, like "*peptide biosynthetic process*" and "*phosphorus metabolic process*". Also, the general "*transport*" term, ends in the more specific term "*amino acid transmembrane export from the vacuole ".*

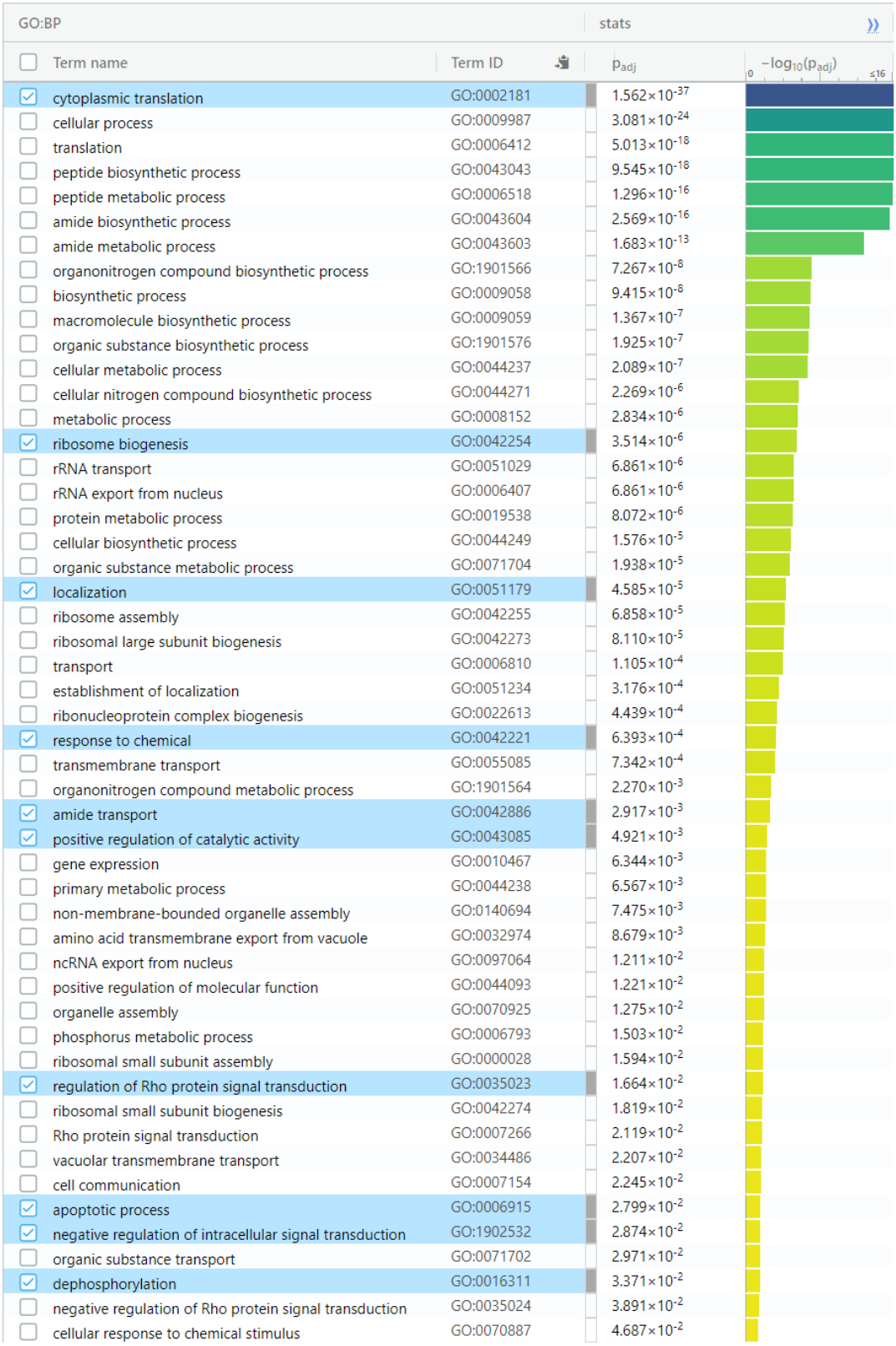

GO:BP		stats
Term name	Term ID	p_{adj}
cytoplasmic translation	GO:0002181	1.562×10^{-37}
cellular process	GO:0009987	3.081×10^{-24}
translation	GO:0006412	5.013×10^{-18}
peptide biosynthetic process	GO:0043043	9.545×10^{-18}
peptide metabolic process	GO:0006518	1.296×10^{-16}
amide biosynthetic process	GO:0043604	2.569×10^{-16}
amide metabolic process	GO:0043603	1.683×10^{-13}
organonitrogen compound biosynthetic process	GO:1901566	7.267×10^{-8}
biosynthetic process	GO:0009058	9.415×10^{-8}
macromolecule biosynthetic process	GO:0009059	1.367×10^{-7}
organic substance biosynthetic process	GO:1901576	1.925×10^{-7}
cellular metabolic process	GO:0044237	2.089×10^{-7}
cellular nitrogen compound biosynthetic process	GO:0044271	2.269×10^{-6}
metabolic process	GO:0008152	2.834×10^{-6}
ribosome biogenesis	GO:0042254	3.514×10^{-6}
rRNA transport	GO:0051029	6.861×10^{-6}
rRNA export from nucleus	GO:0006407	6.861×10^{-6}
protein metabolic process	GO:0019538	8.072×10^{-6}
cellular biosynthetic process	GO:0044249	1.576×10^{-5}
organic substance metabolic process	GO:0071704	1.938×10^{-5}
localization	GO:0051179	4.585×10^{-5}
ribosome assembly	GO:0042255	6.858×10^{-5}
ribosomal large subunit biogenesis	GO:0042273	8.110×10^{-5}
transport	GO:0006810	1.105×10^{-4}
establishment of localization	GO:0051234	3.176×10^{-4}
ribonucleoprotein complex biogenesis	GO:0022613	4.439×10^{-4}
response to chemical	GO:0042221	6.393×10^{-4}
transmembrane transport	GO:0055085	7.342×10^{-4}
organonitrogen compound metabolic process	GO:1901564	2.270×10^{-3}
amide transport	GO:0042886	2.917×10^{-3}
positive regulation of catalytic activity	GO:0043085	4.921×10^{-3}
gene expression	GO:0010467	6.344×10^{-3}
primary metabolic process	GO:0044238	6.567×10^{-3}
non-membrane-bounded organelle assembly	GO:0140694	7.475×10^{-3}
amino acid transmembrane export from vacuole	GO:0032974	8.679×10^{-3}
ncRNA export from nucleus	GO:0097064	1.211×10^{-2}
positive regulation of molecular function	GO:0044093	1.221×10^{-2}
organelle assembly	GO:0070925	1.275×10^{-2}
phosphorus metabolic process	GO:0006793	1.503×10^{-2}
ribosomal small subunit assembly	GO:0000028	1.594×10^{-2}
regulation of Rho protein signal transduction	GO:0035023	1.664×10^{-2}
ribosomal small subunit biogenesis	GO:0042274	1.819×10^{-2}
Rho protein signal transduction	GO:0007266	2.119×10^{-2}
vacuolar transmembrane transport	GO:0034486	2.207×10^{-2}
cell communication	GO:0007154	2.245×10^{-2}
apoptotic process	GO:0006915	2.799×10^{-2}
negative regulation of intracellular signal transduction	GO:1902532	2.874×10^{-2}
organic substance transport	GO:0071702	2.971×10^{-2}
dephosphorylation	GO:0016311	3.371×10^{-2}
negative regulation of Rho protein signal transduction	GO:0035024	3.891×10^{-2}
cellular response to chemical stimulus	GO:0070887	4.687×10^{-2}

Figure 3.13 Upregulated DEGs biological process: *The biological processes of the upregulated differentially expressed genes from contrast (Ca0P05, Ca1P05) used as input in Gprofiler. 497 gene orthologs to yeast are used as input queries. Highlighted terms are driver terms in each component.*

The driver terms in the cell component in upregulated DEGs are "*cytosolic ribosome*" and "*cellular bud*" (Figure 3.14). Almost all terms in the cell components belong to the ribosome, and the making of ribosome. Only two of the terms are not included in ribosome activity, but these are a part of the cellular bud ("*mating projection*" and "*cellular bud neck*").

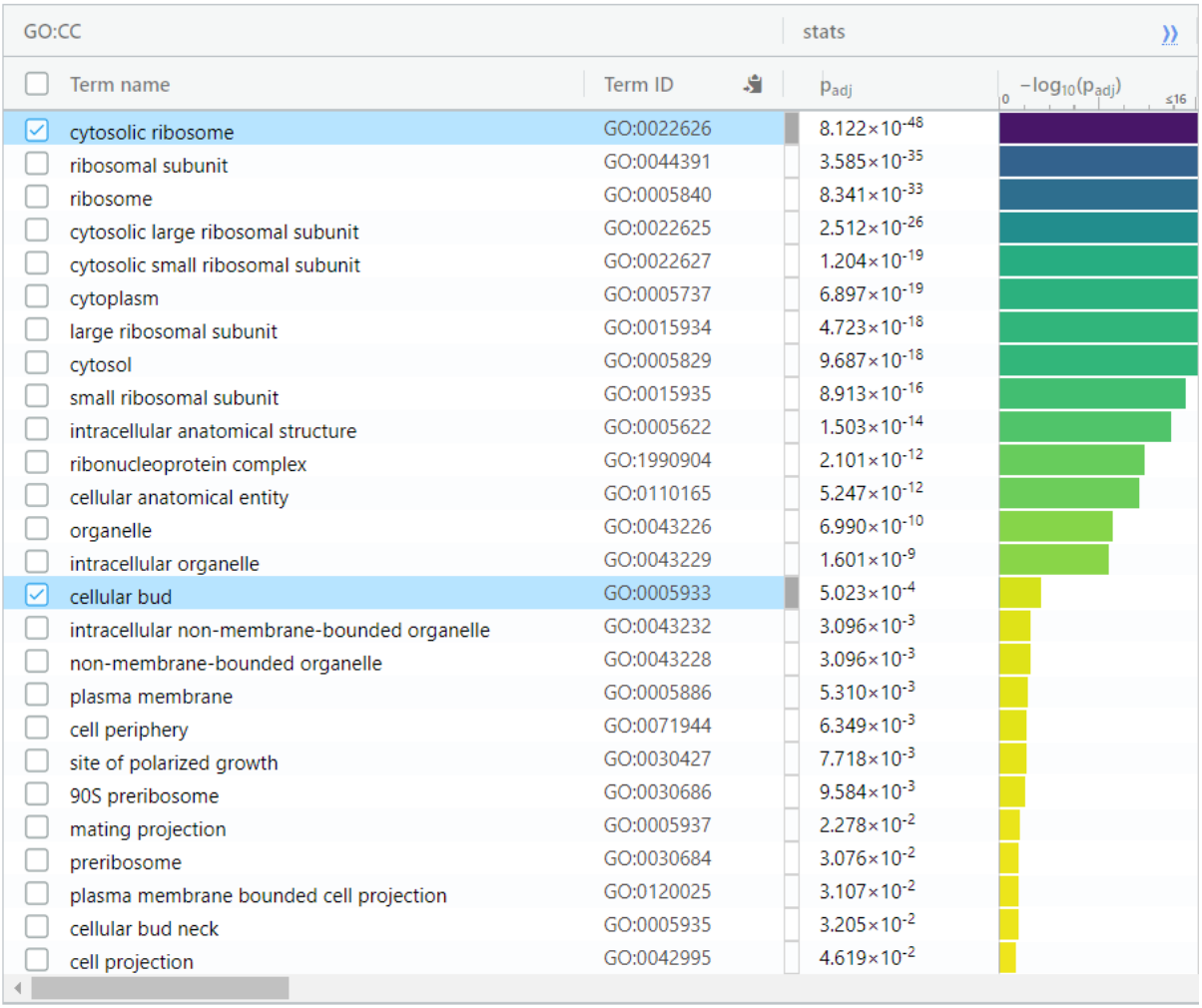

Figure 3.14 Upregulated DEGs cell component: *The cell components of the upregulated differentially expressed genes from contrast (Ca0P05, Ca1P05) used as input in Gprofiler. 497 gene orthologs to yeast are used as input queries. Highlighted terms are driver terms in each component.*

3.7.2 Function of the downregulated DEGs

The driver terms in the molecular function of downregulated DEGs are "*catalytic activity*", "*binding*" and "*catalytic activity, acting on DNA*" (Figure 3.15). Several of the terms are in the peptidase general term and ATP hydrolysis activity. The driver term "binding" has a lot of different more specific terms connected to it, with all except "protein binding" ending in "ATP binding".

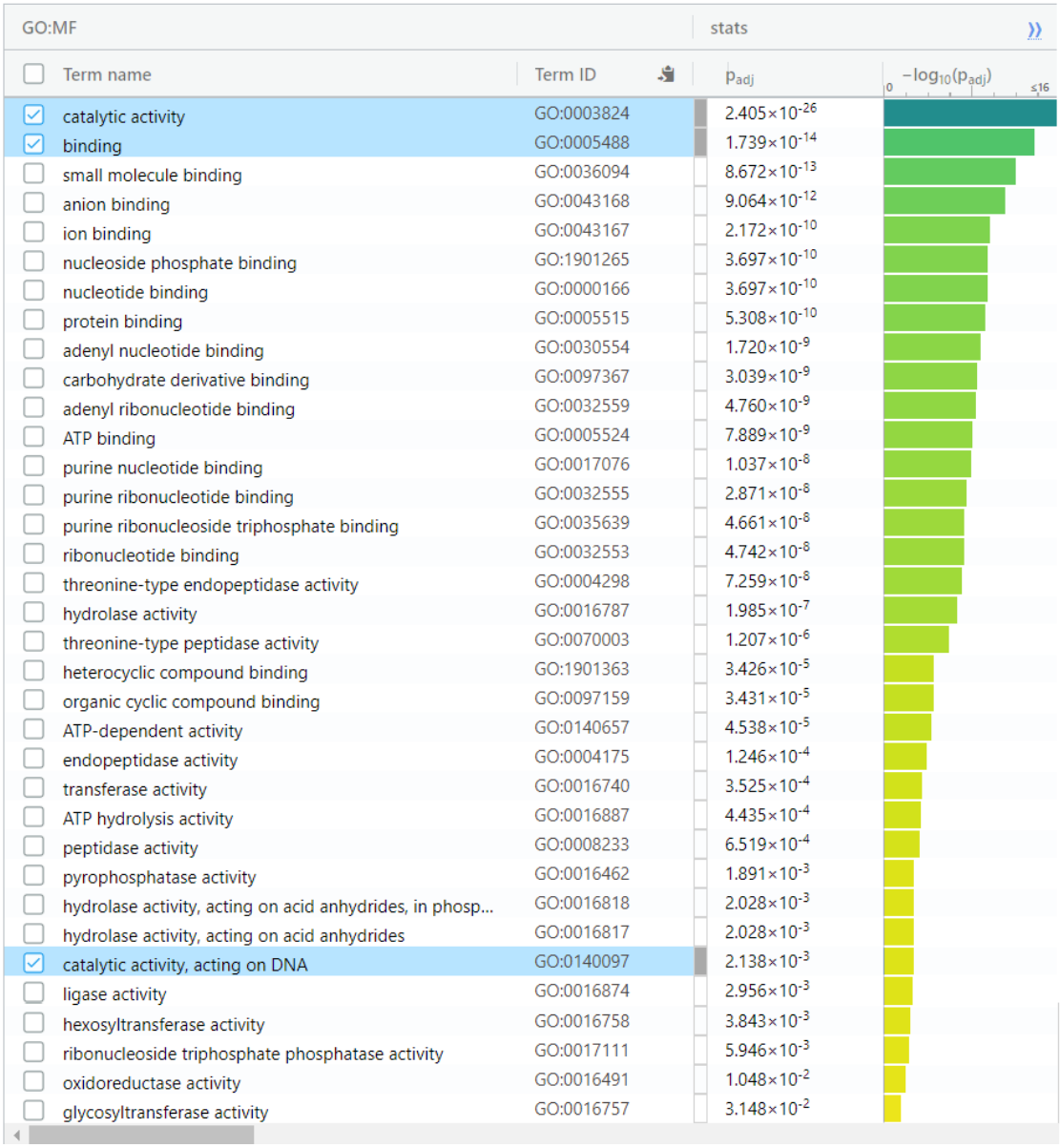

Figure 3.15 Downregulated DEGs molecular function: *The molecular functions of the downregulated differentially expressed genes from contrast (Ca0P05, Ca1P05) used as input in Gprofiler. 497 gene orthologs to yeast are used as input queries. Highlighted terms are driver terms in each component.*

The driver terms in the biological processes in downregulated DEGs are "*organic substance metabolic process*", "*DNA strand elongation*", "*proteasomal ubiquitin-independent protein catabolic process*", "*cellular response to stress*", "*proteasome-mediated ubiquitin-dependent protein carrier*", "*arginine biosynthetic process*", "*proteasome assembly*", "*negative regulation of antisense RNA transcription*", "*regulation of antisense RNA transcription*", "*regulation of ncRNA transcription*" and "*mitotic sister chromatid cohesion*" (Figure 3.16). All the DNA-related terms are connected to the "*response to stimulus*" term. Several of the driver terms are in the proteasome term group.

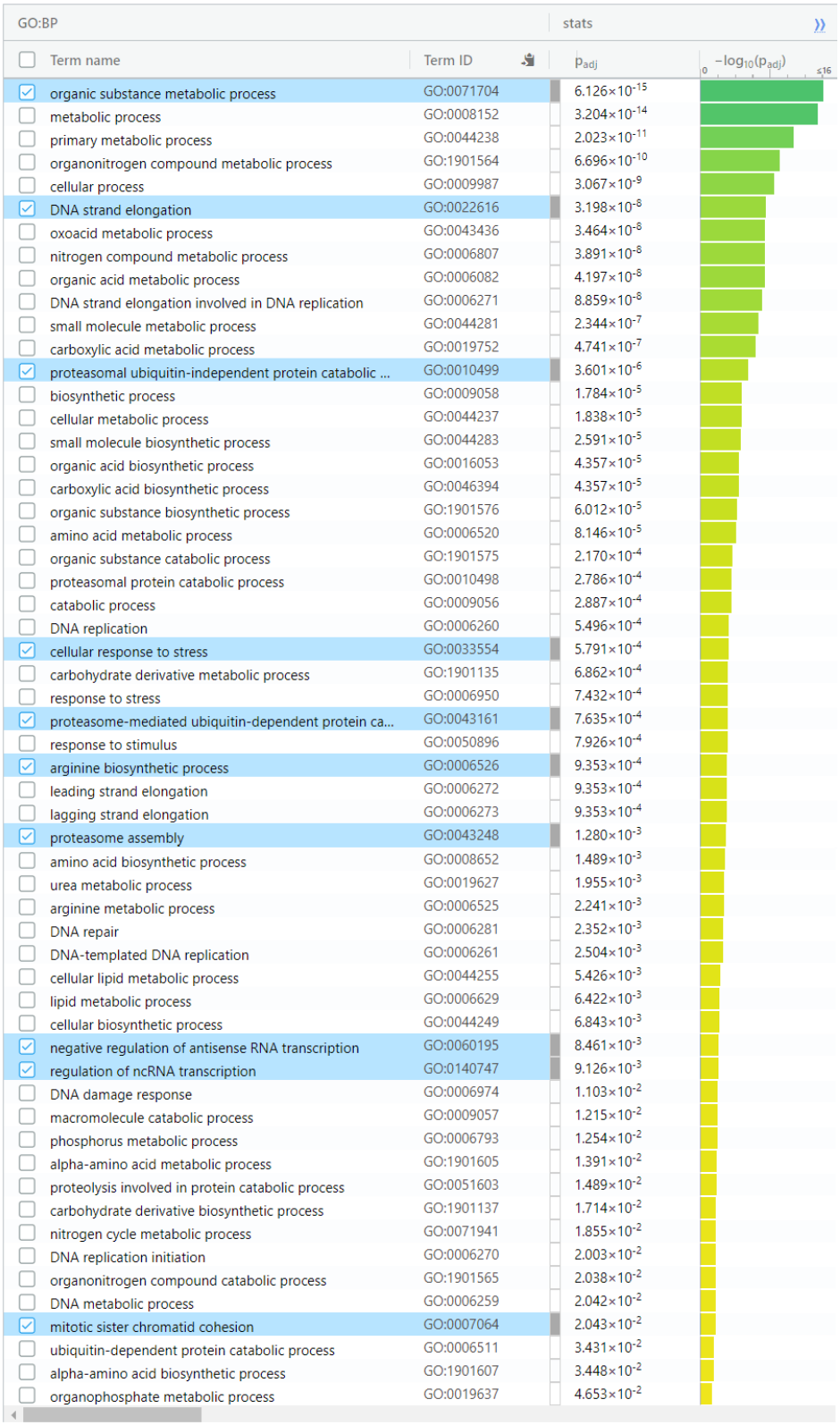

Figure 3.16 Downregulated DEGs biological process: *The biological processes of the downregulated differentially expressed genes from contrast (Ca0P05, Ca1P05) used as input in Gprofiler. 497 gene orthologs to yeast are used as input queries. Highlighted terms are driver terms in each component.*

The driver terms in cell components of downregulated DEGs are "*intracellular anatomical structure*" and "*mitotic cohesin complex*" (Figure 3.17). Several of the downregulated terms are in the proteasome and DNA category, such as in the biological process (Figure 3.16).

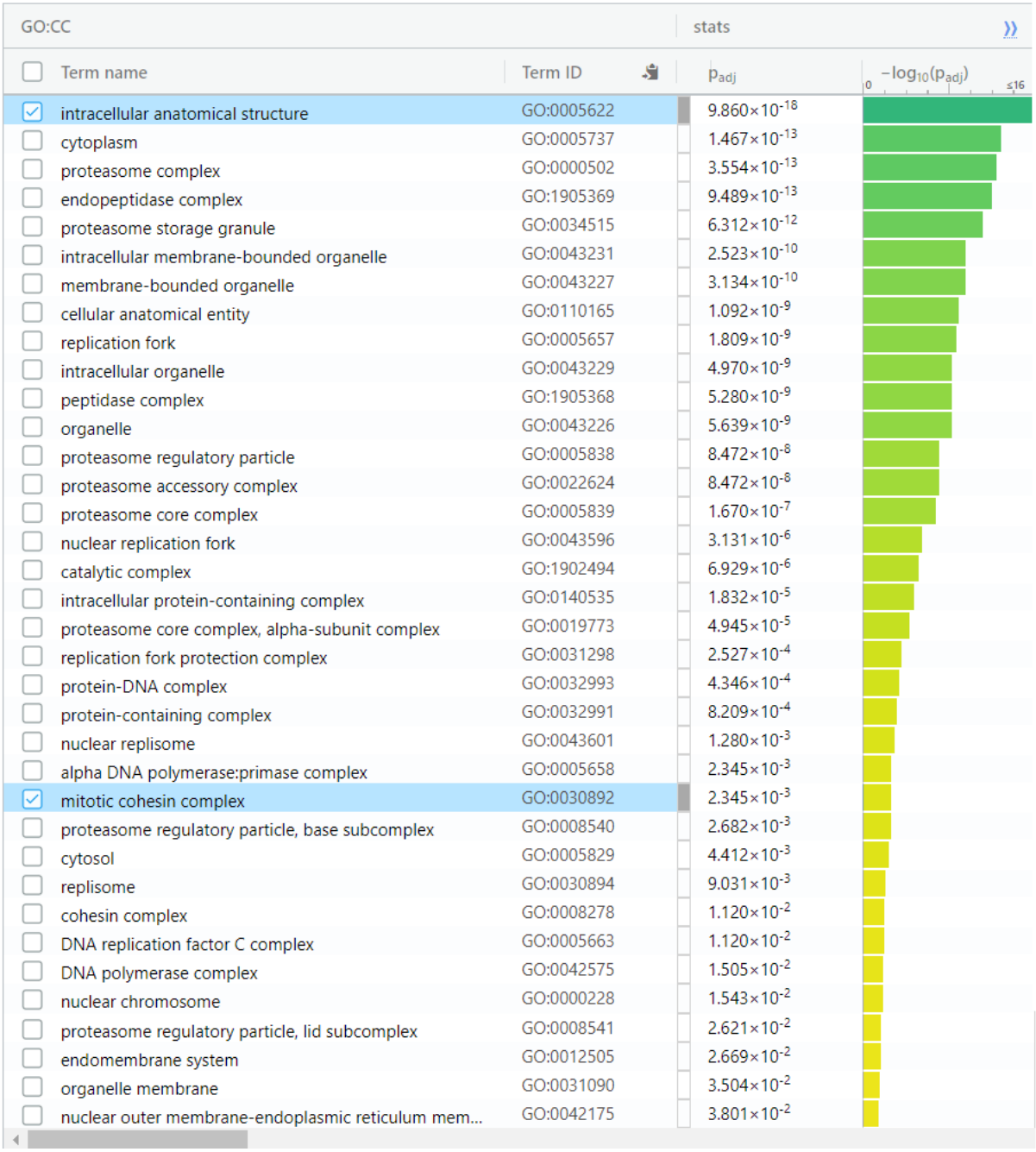

GO:CC		stats	
Term name	Term ID	p_{adj}	$-\log_{10}(p_{adj})$
intracellular anatomical structure	GO:0005622	9.860×10^{-18}	
cytoplasm	GO:0005737	1.467×10^{-13}	
proteasome complex	GO:0000502	3.554×10^{-13}	
endopeptidase complex	GO:1905369	9.489×10^{-13}	
proteasome storage granule	GO:0034515	6.312×10^{-12}	
intracellular membrane-bounded organelle	GO:0043231	2.523×10^{-10}	
membrane-bounded organelle	GO:0043227	3.134×10^{-10}	
cellular anatomical entity	GO:0110165	1.092×10^{-9}	
replication fork	GO:0005657	1.809×10^{-9}	
intracellular organelle	GO:0043229	4.970×10^{-9}	
peptidase complex	GO:1905368	5.280×10^{-9}	
organelle	GO:0043226	5.639×10^{-9}	
proteasome regulatory particle	GO:0005838	8.472×10^{-8}	
proteasome accessory complex	GO:0022624	8.472×10^{-8}	
proteasome core complex	GO:0005839	1.670×10^{-7}	
nuclear replication fork	GO:0043596	3.131×10^{-6}	
catalytic complex	GO:1902494	6.929×10^{-6}	
intracellular protein-containing complex	GO:0140535	1.832×10^{-5}	
proteasome core complex, alpha-subunit complex	GO:0019773	4.945×10^{-5}	
replication fork protection complex	GO:0031298	2.527×10^{-4}	
protein-DNA complex	GO:0032993	4.346×10^{-4}	
protein-containing complex	GO:0032991	8.209×10^{-4}	
nuclear replisome	GO:0043601	1.280×10^{-3}	
alpha DNA polymerase:primase complex	GO:0005658	2.345×10^{-3}	
mitotic cohesin complex	GO:0030892	2.345×10^{-3}	
proteasome regulatory particle, base subcomplex	GO:0008540	2.682×10^{-3}	
cytosol	GO:0005829	4.412×10^{-3}	
replisome	GO:0030894	9.031×10^{-3}	
cohesin complex	GO:0008278	1.120×10^{-2}	
DNA replication factor C complex	GO:0005663	1.120×10^{-2}	
DNA polymerase complex	GO:0042575	1.505×10^{-2}	
nuclear chromosome	GO:0000228	1.543×10^{-2}	
proteasome regulatory particle, lid subcomplex	GO:0008541	2.621×10^{-2}	
endomembrane system	GO:0012505	2.669×10^{-2}	
organelle membrane	GO:0031090	3.504×10^{-2}	
nuclear outer membrane-endoplasmic reticulum mem...	GO:0042175	3.801×10^{-2}	

Figure 3.17 Downregulated DEGs cell component: *The cell components of the downregulated differentially expressed genes from contrast (Ca0P05, Ca1P05) used as input in Gprofiler. 497 gene orthologs to Saccharomyces cerevisiae are used as input queries. Highlighted terms are driver terms in each component.*

3.8 Genes of special interest

3.8.1 Upregulated genes

From the 24 top upregulated DEGs, expression levels across all treatments were investigated to look for genes with exceptionally high expression patterns in Ca0P0.5 (Figure 3.10). This yielded six DEGs of particular interest, however, three of them had no functional annotation (Figure 3.18). Investigation of yeast orthologs as well as protein BLAST searches against non-redundant protein sequences (nr) database with these genes as query sequences were done to investigate functions of these genes (Table 3.2). FUN_005756 is a putative protein of unknown function but is a predicted member of the oligopeptide transporter (OPT) family of membrane transporters, without a proper gene name when looking at the yeast orthologs. From the BLAST search, two putative homologous sequences on other *Mucor* species (*Mucor lusitanicus* and *Mucor ambiguus*) of the FUN_005756 gene were identified with the functions: "OPT oligopeptide transporter protein-domain-containing protein" and "oligopeptide transporter" (Table 3.2). The expression of the gene FUN_005756 is mainly high in the sample groups with calcium not present. Overall, this gene has a high-count number, up to 30 000 in the Ca0P0.5 group. The gene has around 5000 counts in the other two calcium-lacking groups (Figure 3.18a).
FUN_006934 does not have a yeast ortholog, but from the BLAST search it may be homologous to "DNA-binding WRKY transcription factor" in *Mucor lusitanicus* (Table 3.2). The expression of the gene FUN_006934 is high in the Ca0P0.5 group, with a mean normalized count of around 2200. The expression in the group Ca0P1 is also high for this gene with a mean normalized count of around 900 (Figure 3.18b).
FUN_002648 does not have a yeast ortholog, but from the BLAST search it may be homologous to different enzymes; "Isochorismatase family protein", "putative hydrolase" and "nicotinamidase-like amidase" from *Mucor lusitanicus*, and "nicotinamidase family protein YcaC" from *Mucor ambiguus* (Table 3.2). The expression of the gene FUN_002648 is high in Ca0P0.5, and low to non-existent in the other groups (Figure 3.18c).
FUN_009980 has a yeast ortholog gene encoding Hexose transport (*HXT3*) (Figure 3.18d). From the BLAST search, it appears closely related to three sequences of "general substrate transporter" from *Mucor lusitanicus*, *Mucor ambiguus* and *Parasitella parasitica* (Table 3.2). The expression of the gene FUN_009980 is very high in Ca0P0.5, and low to none in the other groups (Figure 3.18d).
FUN_006614 has a yeast ortholog gene encoding SUN domain-containing protein 3 (*SUN3*) (Figure 3.18e). From the BLAST search, two potential homologs of the FUN_006614 gene were detected: "UNC-like-C-terminal-domain-containing protein" and "SUN domain-containing protein" from *Mucor lusitanicus* and *Gilbertella persicaria*, and *Parasitella parasitica* (Table 3.2). The expression of the gene FUN_006614 is very high in Ca0P0.5, and low to none in the other groups (Figure 3.18e).
FUN_008120 does not have a yeast ortholog, but from the BLAST search it may be homologus to part of DNA-binding WRKY transcription factor in *Mucor lusitanicus*, just like FUN_006934 (Table 3.2). The expression of the gene FUN_008120 is very high in Ca0P0.5, and low to none in the other groups (Figure 3.18f).

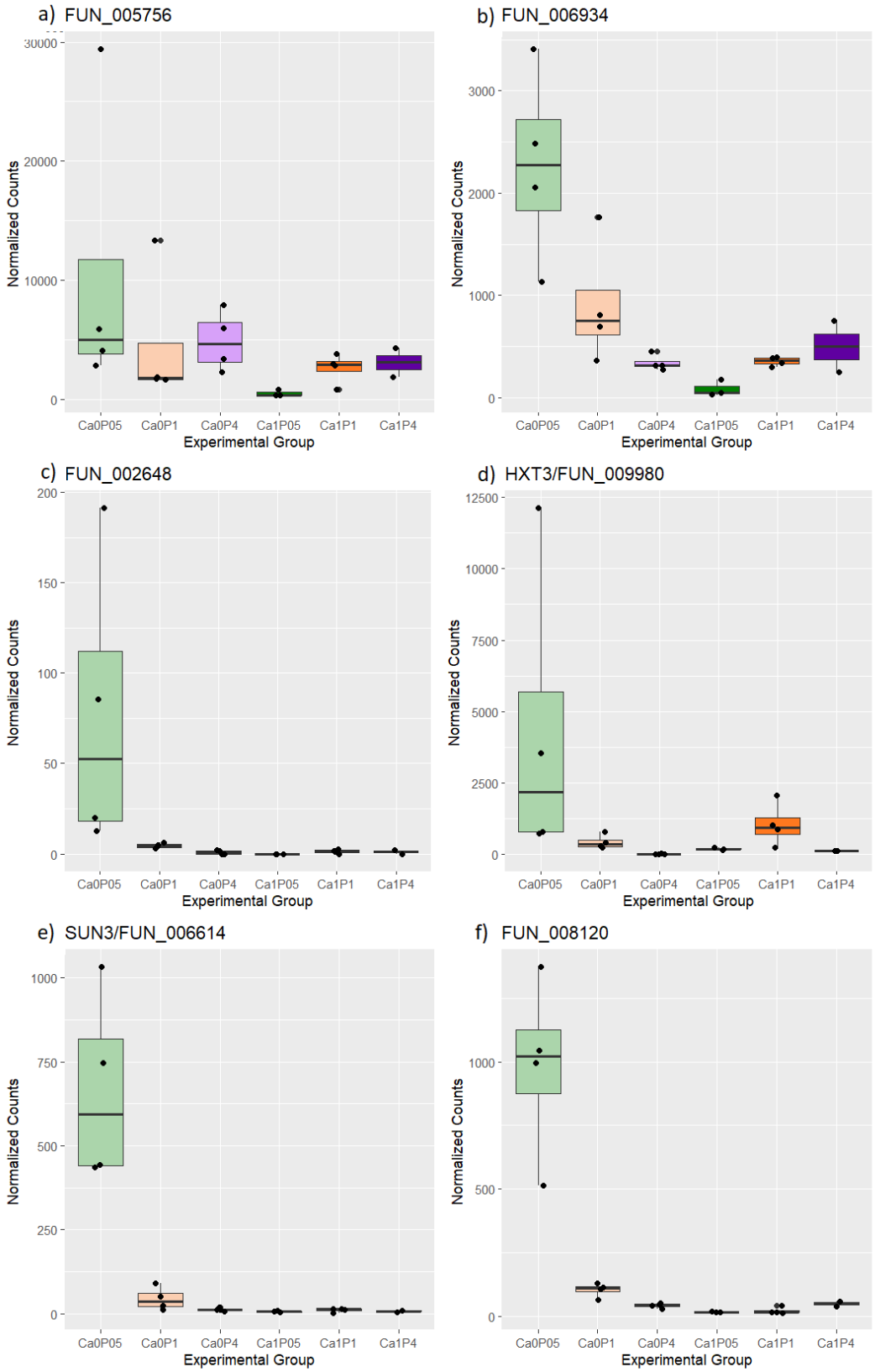

Figure 3.18 Expression of the upregulated genes in Ca0P05 compared to the other treatments: Expression of the normalized counts of the genes, a)*FUN_005756, b)FUN_006934, c)FUN_002646, d)FUN_009980, e)FUN_006614 and f)FUN_008120.*

Table 3.2 Functions of putative homologous genes the upregulated DEGs identified with BLAST: *Possible gene descriptions for the genes, FUN_005756, FUN_006934, FUN_002646, FUN_009980, FUN_006614 and FUN_008120, and which organism the aligned function comes from.*

GeneID	Gene description:	Organism:
FUN_005756	OPT oligopeptide transporter protein-domain-containing protein	*Mucor lusitanicus, Parasitella parasitica, Benjaminiella poitrasii, Mycotypha africana, Gilbertella persicaria*
	Oligopeptide transporter	*Mucor ambiguus*
FUN_006934	DNA-binding WRKY transcription factor	*Mucor lusitanicus* CBS 277.49 *Mucor lusitanicus*
	Isochorismatase family protein	*Mucor lusitanicus, Mucor lusitanicus*
FUN_002648	Nicotinamidase family protein YcaC	*Mucor ambiguus*
	Putative hydrolase	*Mucor lusitanicus*
	Nicotinamidase-like amidase	*Mucor lusitanicus*
FUN_009980	General substrate transporter	*Mucor lusitanicus, Mucor lusitanicus, Mucor ambiguus, Parasitella parasitica*
FUN_006614	UNC-like C-terminal-domain-containing protein	*Mucor lusitanicus, Gilbertella persicaria*
	SUN domain-containing protein	*Parasitella parasitica*
FUN_008120	DNA-binding WRKY transcription factor	*Mucor lusitanicus* CBS 277.49 *Mucor lusitanicus*

3.8.2 Downregulated genes

From the 14 top downregulated DEGs (Figure 3.10), expression levels across all treatments were investigated to look for genes with exceptionally low expression patterns in Ca0P0.5. This yielded six DEGs of particular interest, however, four of them had no functional annotation (Figure 3.19). Investigation of yeast orthologs as well as BLAST searches against non-redundant protein sequences (nr) database with these genes as query sequences were done to investigate functions of these genes (Table 3.3).

FUN_006499 has a yeast ortholog, *ICL1_2* encoding isocitrate lyase 1. This is confirmed by BLAST hits against homologous genes in other species (Table 3.3). The expression of the gene FUN_006499 is zero in Ca0P0.5 and varies significantly from low to high in the other treatments (Figure 3.19a).
FUN_6192 does not have a yeast ortholog but from the BLAST search (Table 3.3) it may be homologous to two methyltransferases; type 11 methyltransferase in *Mucor ambiguus* and S-adenosyl-L-methionine-dependent methyltransferase aligned in *Mucor lusitanicus* and *Parasitella parasitica*. The expression of the gene FUN_006192 is zero in Ca0P0.5, high in Ca0P1, Ca1P1, Ca1P0.5 and moderately expressed in Ca0P4 and Ca1P4 (Figure 3.19b) .
FUN_003609 and FUN_008998 do not have yeast orthologs, and top 100 BLAST hits only against hypothetical proteins in other species (Table 3.3). The expression of the gene FUN_003609 is zero in Ca0P0.5, very high in Ca0P1 and moderate in the other groups (Figure 3.19c).
The expression of the gene FUN_008998 is zero in Ca0P0.5, very high in groups with calcium, and moderate in Ca0P1 and Ca0P4 (Figure 3.19e).
FUN_004498 does not have a yeast ortholog, but from the BLAST search it may be homologous to a coth protein-domain-containing protein, found in several species (Table 3.3). The expression of the gene FUN_004498 is zero in Ca0P0.5, and generally high in groups with calcium, and medium in Ca0P1 and Ca0P4 (Figure 3.19d).
FUN_011893 has a yeast ortholog, *LYS2* encoding Alpha aminoadipate reductase. It is putatively homologous to *SmoA* and *SmoF* in *Mucor circinelloides*, encoding Acetyl-CoA synthetase (AMP-forming)/AMP-acid ligase II, and L-aminoadipate-semialdehyde dehydrogenase (*LYS5*) in *Mucor ambiguous* (Table 3.3). Further investigation on which gene function is the right one is needed, however, both have functions to do with Acetyl-CoA, which is a well-known component of the carotenoid biosynthetic pathway (Figure 1.1). The expression of the gene FUN_011893 is zero in Ca0P0.5, zero to none in Ca0P1, Ca0P4, Ca1P1, Ca1P4, and very high in Ca1P0.5 (Figure 3.19f).

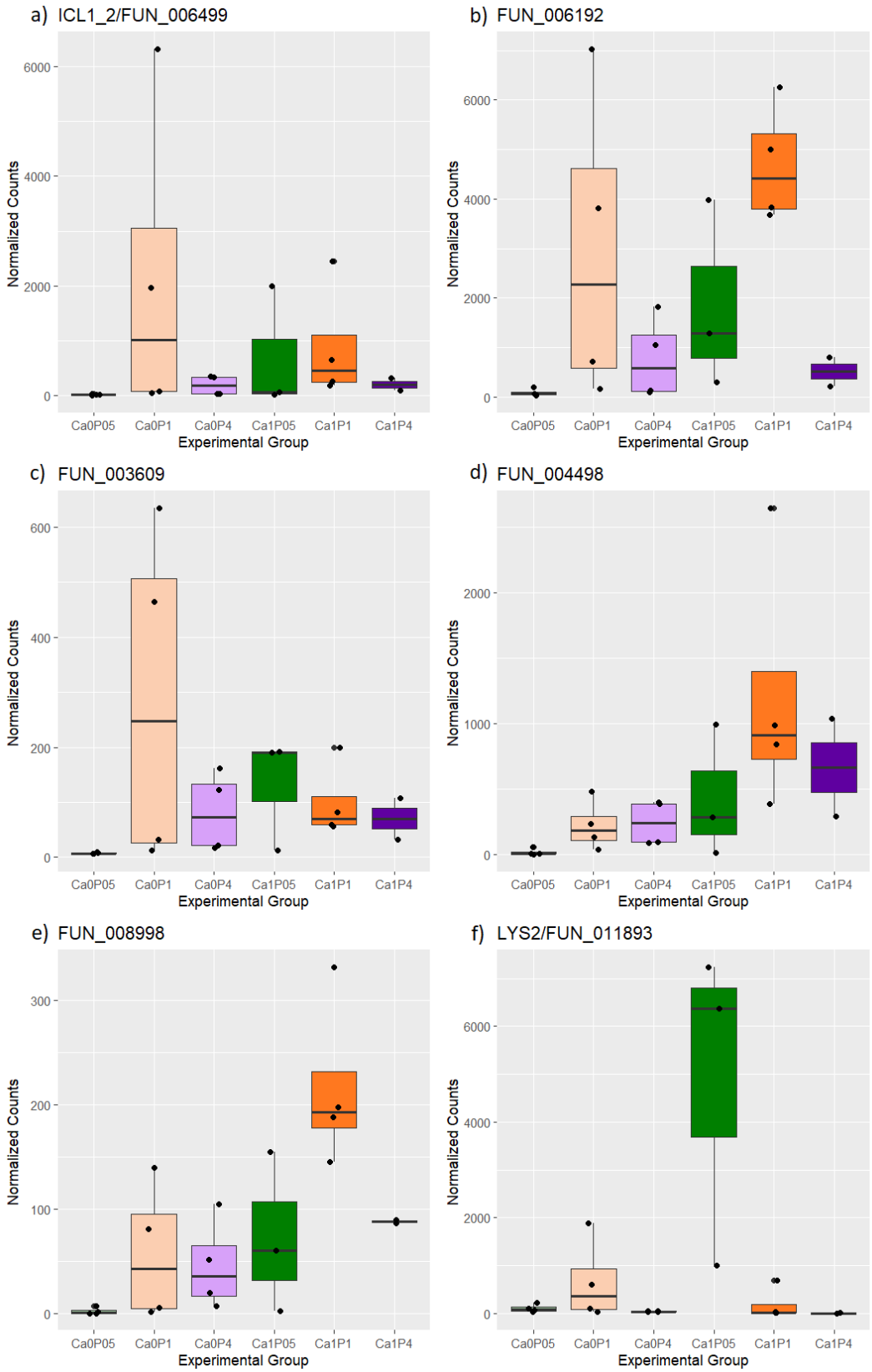

Figure 3.19 Expression of top downregulated DEGs in Ca0P05 compared to the other treatments: *Expression of the normalized counts of the genes, a) FUN_006499, b)FUN_006192, c)FUN_003609, d)FUN_004498, e)FUN_008998 and f)FUN_011893.*

Table 3.3 ***Aligned functions of putative homologous genes the downregulated DEGs identified with BLAST:*** *Possible gene descriptions for the genes, FUN_006499, FUN_006192, FUN_003609, FUN_004498, FUN_008998 and FUN_011893, and which organism the aligned function comes from.*

GeneID	Gene description:	Organism:
FUN_006499	Isocitrate lyase	*Mucor circinelloides 1006PhL, Mucor lusitanicus, Mucor ambiguus, Parasitella parasitica, Mucor mucedo, Mycotypha africana, Blakeslea trispora*
FUN_006192	Type 11 methyltransferase	*Mucor ambiguus*
	S-adenosyl-L-methionine-dependent methyltransferase	*Mucor lusitanicus, Parasitella parasitica*
FUN_003609	NA	*NA*
FUN_004498	Coth protein-domain-containing protein	*Mucor lusitanicus, Parasitella parasitica, Benjaminiella poitrasii, Blakeslea trispora, Choanephora cucurbitarum, Thamnidium elegans*
FUN_008998	NA	*NA*
FUN_011893	SmoA	*Mucor circinelloides*
	L-aminoadipate-semialdehyde dehydrogenase	*Mucor ambiguus*
	SmoF	*Mucor circinelloides*

3.9 Candidate genes

Sequences for candidate genes for carotenoid production were BLASTed against the annotated genes in *Mucor circinelloides* to identify homologous genes in this species (Table 3.4). Ten putative homologs were identified and investigated further. Only two of them were putatively homologous to significant DEGs.
The *carG* (geranylgeranyl pyrophosphate synthase) gene is homologous to FUN_009191 and is significantly downregulated with a log2FoldChange of -2,458893 (Table 3.4). The expression of FUN_009191 is low in Ca0P0.5, Ca0P4 and Ca1P4, medium in Ca1P0.5, high with lots of variance in Ca0P1, and high with low variance in Ca1P1 (Figure 3.20a).

The *crgA* (carotenoid regulatory protein) gene is homologous to FUN_0010938 and FUN_007660. FUN_007660 is significantly downregulated with a log2FoldChange of -2,045957 (Table 3.4) The expression of FUN_007660 is low in Ca0P0.5 and Ca0P4, and high in the other treatment. The normalized count is in general exceptionally high compared to other DEGs with the highest count of the gene around 80 000 (Figure 3.20b).

For the remaining candidate genes, *carB*, *carRP*, *hmgR2* and *hmgR3* no homologous genes that were significantly differentially expressed were identified. However, for the matching homolog FUN_005064 for *hmgR2* and *hmgR3* and the homolog FUN_010046 for *carRP* have p-adj values of 0.06 and 0.09, respectively. *HmgR2* and *hmgR3* encodes HMG-CoA reductase, and *carRP* encodes lycopene cyclase/phytoene synthase (Figure 3.4).

Table 3.4 Aligned genes to the candidate genes in BLAST and if they are differentially expressed: *candidate genes for carotenoid production in Mucor circinelloides and aligned geneID, with their bits score and E value. Differentially expressed genes have their respectively p-adjust and Log2FoldChange value present.*

BLAST				DEGs	
Function:	**GeneID:**	**Score (Bits):**	**E Value:**	**P-adj:**	**Log2FC:**
phytoene dehydrogenase [Mucor circinelloides 1006PhL] **(carB)**	FUN_010047	1204	0.0	0.29224949	-1.52896330
phytoene dehydrogenase [Phycomyces blakesleeanus] **(carB)**	FUN_010047	886	0.0	0.29224949	-1.52896330
geranylgeranyl pyrophosphate synthase [Mucor lusitanicus] **(carG)**	FUN_000732	613	0.0	0.23518787	-1.19921438
	FUN_009191	425	5e-151	**0.03992117**	**-2.458893**
carotenoid regulatory protein [Mucor circinelloides] **(crgA)**	FUN_010938	174	2e-47	0.91528937	0.12694736
	FUN_007660	99,4	2e-22	**0.02623850**	**-2.045957**
lycopene cyclase/phytoene synthase [Phycomyces blakesleeanus] **(carRP)**	FUN_010046	703	0.0	0.09300939	-2.43795133
	FUN_004555	192	8e-54	0.88526259	0.21549360
HMG-CoA reductase 2, partial [Mucor lusitanicus] **(hmgR2)**	FUN_005064	1061	0.0	0.06200890	1.00649705
	FUN_006897	1060	0.0	0.35085130	0.41960638
	FUN_005802	839	0.0	0.97739187	-0.02196950
HMG-CoA reductase 3, partial [Mucor lusitanicus] **(hmgR3)**	FUN_005064	2118	0.0	0.06200890	1.00649705
	FUN_005802	1026	0.0	0.97739187	-0.02196950
	FUN_006897	841	0.0	0.35085130	0.41960638

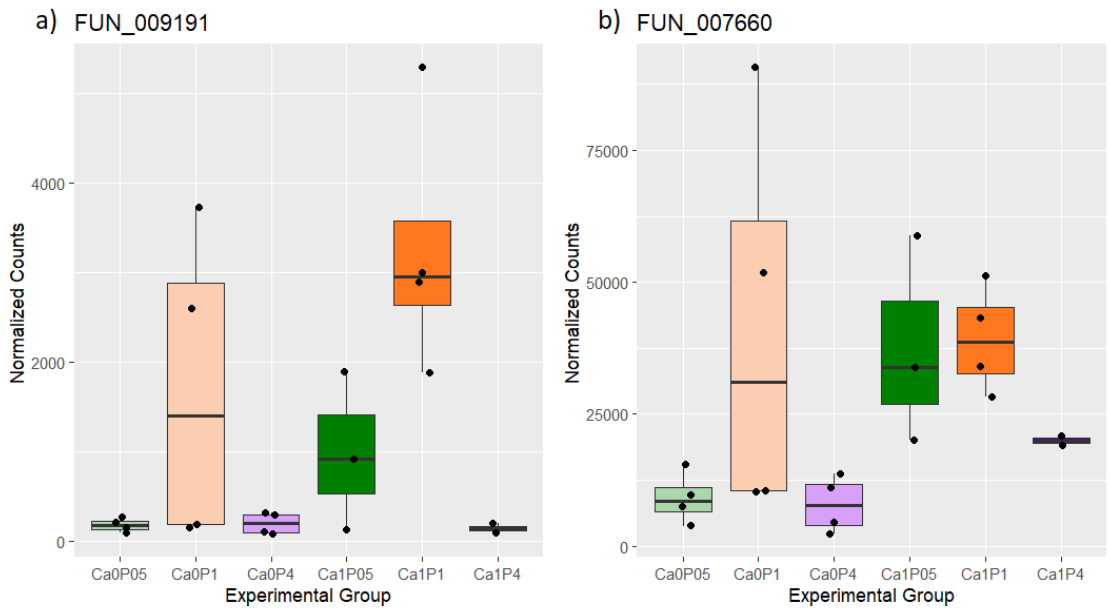

Figure 3.20 Expression of the candidate genes, which are differentially expressed: *a) CarG (FUN_009191) and b) CrgA (FUN_007660).*

4 Discussion

In this thesis I have examined the effect of calcium on carotenoid production in *Mucor circinelloides*. By investigating how calcium and phosphorus starvation affects gene expression and phenotypes of this fungus, I have identified genes that both directly and indirectly influence the carotenoid pathway under different calcium conditions. In the following discussion, I will first address the indirect effects, and then the direct effects on the carotenoid pathway in *Mucor circinelloides.* Finally, I will discuss the future implications of these findings.

4.1 Effect of calcium

4.1.1 Indirect effect of calcium on the carotenoid pathway

The function of the upregulated genes from the GO enrichment analysis is mostly connected to protein synthesis, through either ribosomal activity or direct peptide biosynthetic processes, and some genes are connected to dimorphic switching through an upregulation of the budding cell division (Figure 3.14). This could imply that calcium has an indirect effect on the carotenoid pathway through protein synthesis and affects dimorphic switching in *Mucor circinelloides* (Figure 4.1a).

It was reported in a study on eukaryotic cells that calcium serves as a physiological regulator of post-transcriptional protein synthesis (Brostrom et al., 1986). The effect of calcium ion on protein synthesis have largely been seen in intact cells or tissues exposed to low extracellular calcium concentration such as the depletion of intracellular calcium stores occurs with a concomitant 4-10 fold reduction in the rate of amino acid incorporation (Chin et al., 1987). Chin et al. presents evidence in support of the proposal that calcium affects mRNA translation at initiation rather than peptide chain elongation or termination in eukaryotic cells. In the Chin et al. study it was observed an effect of calcium on ribosomal subunit, monosomal, and polysomal contents and also on average ribosomal transit times. They found out that cells exposed to calcium for 5 min, in contrast to the calcium depleted cells, were sharply reduced in their contents of ribosomal subunits, meaning that possible genes associated with ribosomes function and activity were downregulated in the presence of calcium. This research complements the results from my study, with the upregulation of ribosomes on the calcium depleted cell.
Further, the upregulation of ribosomes affects the protein synthesis. The change in protein activity may influence the carotenoid production, like it was proposed in the review article, (Sandra et al., 2017), changes in protein activity affects the pigment production by affecting pH and temperature. This was also proposed by (Gmoser et al., 2017), due to the strong effect of pH on the biosynthesis of pigments in *Monascus spp.*, and this proposed being associated with changes in the protein activities. Low phosphorus leads to lower pH, and with the driving force of protein synthesis on pH, a more acidic culture condition can be in favor of carotenoid synthesis. Gemoser et al. mention that changing the pH from neutral or slightly alkaline to a more acidic has been shown to favor the cycliation of lycopene to β-carotene.

Another protein connected to carotenoids are the carotenoid regulatory protein, one protein that acts as a negative regulator of light-inducible carotenogenesis in *M. circinelloides* (Navarro et al., 2001). The *crgA* gene encoding this protein is significantly downregulated in Ca0P0.5, and the effect of this gene being downregulated is more carotenoids being synthesized.

Genes encoding Rho protein signal transduction (Rho GTPases) is significantly upregulated in the treatment Ca0P0.5 (Figure 3.13). Rho proteins are homologous to the Ras superfamily, which are priorly connected to have a clear influence on dimorphic switching in another fungi, namely *P. brasiliensis*. This switching is regulated by the Ras GTPases by controlling actin-mediated polarized growth and signaling pathways required for morphological responses (Boyce & Andrianopoulos, 2015).

In my study genes related to cell budding were upregulated in samples grown on Ca0 meaning that more yeast-like cells were produced under this condition in comparison to Ca1 condition (Figure 3.14). One regulator of cell morphology and dimorphic switching, together with Rho proteins are calcineurin. Calcineurin is a calcium/calmodulin-dependent, serine/threonine-specific protein phosphatase involved in morphogenesis and virulence of *Mucor* fungi (Lee et al., 2013). Calcineurin is present in many cellular processes and has affinity to more than 200 substrates in the cell. When calcium ions are not present, like in the Ca0 treatment, no activation of calcineurin happens. *Mucor* mutants that lack the calcineurin regulatory subunit essential for calcineurin activity, are locked in perpetual yeast phase growth, indicating that calcineurin is required for hyphal growth and the dimorphic switch (Lee et. al. 2013). Research done on dimorphic switch and carotenoid production in another *Mucor* fungi (*Mucor rouxii*), suggest that yeast like cells usually have less pigmentation then the hyphal cells (Mosqueda-Cano & Gutiérrez-Corona, 1995). The results from yeast-like cells in *Mucor rouxii*, are the opposite from the results in this study. However, we lack quantification on the ratio between hyphal and yeast cells grown, so this needs further investigation.

4.1.2 Direct effect of calcium on the carotenoid pathway

I found a direct effect of calcium starvation influencing gene expression of several genes in the carotenoid pathway (Figure 4.1b). Firstly, we observed that calcium influences the Acetyl-CoA synthase. The genes *smoA* and *smoF* encodes Acetyl-CoA synthase are significantly downregulated (Figure 3.19, Table 3.3), creating a blockage in the carotenoid biosynthesis through the Acetyl-CoA pathway (Figure 4.1b). An indication of this blockage is also through the upregulated genes *hmgR2* and *hmgR3*, which encodes HMG-CoA reductase (Table 3.4). The HMG-CoA is present in the Acetyl-CoA pathway to produce MVAPP used further in the synthesis of carotenoids. The acetyl-CoA pathway uses an extensive amount of ATP, when this part of the biosynthesis is downregulated, ATP is no longer needed in huge amounts, causing a natural downregulation of the ATP hydrolysis (Figure 3.15).

Secondly, calcium influences the hydrolysis of IPP by downregulating pyrophosphatase. Pyrophosphatase is an enzyme that is responsible for the reversible hydrolysis of the phosphoanhydride bond in pyrophosphate (PP_i) to two inorganic phosphate molecules (Li et al., 2020). The effect of this hydrolysis not being present is a congestion of IPP. IPP have two possible pathways to continue in, either be transformed to DAMPP or go directly to the carotenoid biosynthesis (Figure 4.1b).

Thirdly, calcium starvation also led to the downregulation *carB* gene encoding GGPP (Table 3.4). GGPP is a precursor of C40 (orange/red, (Doukani et al., 2022; Kong et al., 2010), C50 (red[7]) and C60 (purple, (Saraswati et al., 2019)) carotenoids. The *carRP* gene, encoding lycopene cyclase/phytoene synthase, is also downregulated, but with the p-adj value at 0.09 (Table 3.4). Phytoene is the precursor of C40 carotenoid, and a product from GGPP. This is another identification of the C40 carotenoid not being present, together with the downregulation of GGPP. The blocked synthesis of C40, C50 and C60 carotenoids leads to a congestion of GPP, which then only have the possibility to be synthesized to C30 carotenoids, which have a yellow color (Umeno et al., 2002). Indeed, the color of the CaP0.5 samples do appear yellow (Figure 3.3), giving plausibility to the hypothesis that calcium starvation leads to an increased production of C30 carotenoids. This would need to be confirmed by quantifying which specific carotenoids are present in the biomass of each sample from each treatment.

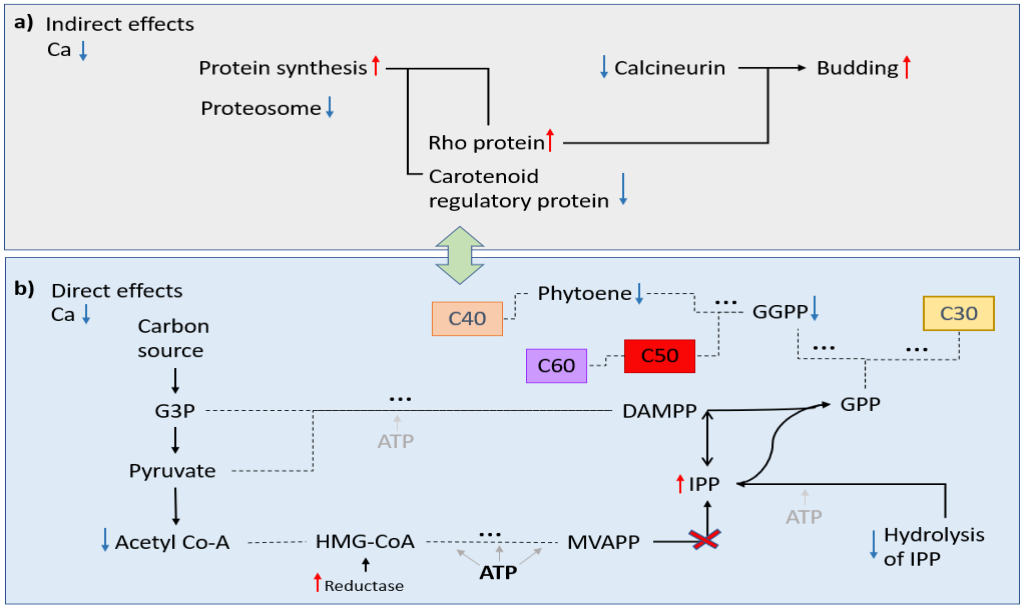

Figure 4.1 The effect of calcium's effect on the carotenoid biosynthesis in Mucor Circinelloides: *a.) shows indirect effects and b.) shows direct effects on carotenoid production, respectively. Pathways in a.) are based on figure 1.1 from (Li et al., 2020). Dotted lines indicate multiple steps in the pathway not shown for simplicity. Red arrows indicate upregulation, blue arrows indicate downregulation. Cross indicates a blocked pathway.*

[7] https://pubchem.ncbi.nlm.nih.gov/compound/Bacterioruberin, accessed 12.05.23

4.2 Future implications

For future implications it would be interesting to find out what kind of carotenoids that are present in the different treatments, to test if the hypothesis of the yellow C30 carotenoids being the dominant carotenoid produced as a result of calcium starvation.

In this study we only examined one strain of *Mucor circinelloides.* By looking at different strains of *Mucor circinelloides*, it would be possible to investigate whether genetic variation between strains could be related differences in terms of carotenoid production with the same treatment. This could be expanded by investigating other Mucoromycota species as well, especially looking at the genetic variation from the different species and strains from the Dzurendova study (Dzurendova et al., 2021). This could contribute to the knowledge of the effect calcium have on carotenoid production, or maybe suggest that the FRR 5020 strain is different enough from the other strains and therefore could be classified as a separate species or subspecies of *Mucor circinelloides*. Indeed, the study done on the subspecies *M. circinelloides f. circinelloides*, *M. circinelloides f. lusitanicus*, and *M. circinelloides f. griseocyanus*, which was suggested that was different enough to be three distinct species, demonstrates the uncertainty regarding phylogenetic relationships in this genus (Lee et al., 2014; Wagner et al., 2020).

It would be interesting to see how the carotenoid production is affected by gene duplication, which can greatly confound analyses of gene expression (Brohard-Julien et al., 2021). The *hmgR2* and *hmgR3* genes have three gene duplications, therefore having a study finding out how similar they are, and how they are regulated would contribute to the understanding of the genetic basis in carotenoid production. Mapping other gene-duplications and connecting these to genetic variation in the different strains could be a future study.

Using CRISPR knock-out to see the function of the genes in the pathway could contribute to the knowledge of the importance of each gene, and the function of the unannotated genes. Especially focusing on the top genes without any homologs, or the genes of which have several different functions annotated (Li et al., 2022; Szebenyi et al., 2023; Trieu et al., 2017) The genome assembly and annotation produced in this study will greatly benefit any CRISPR based studies in the future.

Some studies on carotenoid production have used light regulation as a main trigger for carotenoid production in *Mucor circinelloides* (Navarro et al., 2001; Naz et al., 2020; Silva et al., 2006). Testing if different light conditions on the two treatments (Ca0P0.5 and Ca1P0.5) would change the amount of carotenoids produced, and produce even more carotenoids would be one of the ways to optimize the carotenoid production for biotechnological applications. Connecting the upregulated protein synthesis directly to the carotenoid pathway, by testing if the media after cultivation have a changed pH and compare this to other studies on pH, proteins and carotenoids (Nelis & De Leenheer, 1991; Sandra et al., 2017).

Due to the lack of functional studies in *Mucor* species, the proportion of genes with known function is low (Figure 3.11). The yeast orthologs is not enough to describe every gene in *Mucor circinelloides*. This greatly hampers biological interpretation of gene expression data and is a bottleneck in most studies of gene expression.

5 Conclusion

In this thesis we grew *Mucor circinelloides* under six different treatments to see the effect of calcium and phosphorus on carotenoid production. We used spectroscopy and chromatography to quantify the relative content of lipids and carotenoids, and used gene expression data to examine the genetic basis in carotenoid production.

The testing of relative carotenoid content proved that there was a difference between the different treatments. When *Mucor circinelloides* was grown in the presence and absence of calcium with low phosphorus, it resulted in the highest content of carotenoids. These results were examined further by differential gene expression analysis, to look for genes connected to the carotenoid biosynthetic pathway. The gene expression data indicate that calcium starvation has both an indirect and a direct effect on the biosynthetic pathway of carotenoids.

Most of the upregulated genes affected the general protein synthesis. Genes for dimorphic switching come most likely from the lack of calcineurin activation, the upregulation of Rho protein and as a stress response. The downregulated genes *smoA* and *smoF*, and the candidate upregulated genes *hmgR2* and *hmgR3*, indicate that the Actyl-CoA pathway to carotenoids is downregulated. The downregulated pyrophosphatase genes lead to an increase in IPP, which can be used further in carotenoid biosynthesis. Downregulation of both *carB* and *carRP*, leads to the possibility that production of C30 carotenoids are the most common carotenoid in this fungi.

6 References

Altschul, S. F., Gish, W., Miller, W., Myers, E. W., & Lipman, D. J. (1990). Basic local alignment search tool. *J Mol Biol*, *215*(3), 403-410. https://doi.org/10.1016/s0022-2836(05)80360-2

Ashokkumar, V., Flora, G., Sevanan, M., Sripriya, R., Chen, W. H., Park, J.-H., Rajesh banu, J., & Kumar, G. (2023). Technological advances in the production of carotenoids and their applications– A critical review. *Bioresource Technology*, *367*, 128215. https://doi.org/https://doi.org/10.1016/j.biortech.2022.128215

Botha, A., & Botes, A. (2014). Mucor. In C. A. Batt & M. L. Tortorello (Eds.), *Encyclopedia of Food Microbiology (Second Edition)* (pp. 834-840). Academic Press. https://doi.org/https://doi.org/10.1016/B978-0-12-384730-0.00228-7

Boyce, K. J., & Andrianopoulos, A. (2015). Fungal dimorphism: the switch from hyphae to yeast is a specialized morphogenetic adaptation allowing colonization of a host. *FEMS Microbiology Reviews*, *39*(6), 797-811. https://doi.org/10.1093/femsre/fuv035

Brohard-Julien, S., Frouin, V., Meyer, V., Chalabi, S., Deleuze, J.-F., Le Floch, E., & Battail, C. (2021). Region-specific expression of young small-scale duplications in the human central nervous system. *BMC Ecology and Evolution*, *21*(1), 59. https://doi.org/10.1186/s12862-021-01794-w

Brostrom, C. O., Bocckino, S. B., Brostrom, M. A., & Galuska, E. M. (1986). Regulation of protein synthesis in isolated hepatocytes by calcium-mobilizing hormones. *Molecular Pharmacology*, *29*(1), 104-111. https://molpharm.aspetjournals.org/content/molpharm/29/1/104.full.pdf

Candan, N., & Tarhan, L. (2005). Effects of Calcium, Stress on Contents of Chlorophyll and Carotenoid, LPO Levels, and Antioxidant Enzyme Activities in Mentha. *Journal of Plant Nutrition*, *28*(1), 127-139. https://doi.org/10.1081/PLN-200042192

Chen, Y., Zhang, Y., Wang, A. Y., Gao, M., & Chong, Z. (2021). Accurate long-read de novo assembly evaluation with Inspector. *Genome Biology*, *22*(1), 312. https://doi.org/10.1186/s13059-021-02527-4

Chin, K. V., Cade, C., Brostrom, C. O., Galuska, E. M., & Brostrom, M. A. (1987). Calcium-dependent regulation of protein synthesis at translational initiation in eukaryotic cells. *Journal of Biological Chemistry*, *262*(34), 16509-16514. https://doi.org/https://doi.org/10.1016/S0021-9258(18)49285-X

Chiou, C. Y., Pan, H. A., Chuang, Y. N., & Yeh, K. W. (2010). Differential expression of carotenoid-related genes determines diversified carotenoid coloration in floral tissues of Oncidium cultivars. *Planta*, *232*(4), 937-948. https://doi.org/10.1007/s00425-010-1222-x

Clapham, D. E. (2007). Calcium Signaling. *Cell*, *131*(6), 1047-1058. https://doi.org/https://doi.org/10.1016/j.cell.2007.11.028

Dobin, A., Davis, C. A., Schlesinger, F., Drenkow, J., Zaleski, C., Jha, S., Batut, P., Chaisson, M., & Gingeras, T. R. (2013). STAR: ultrafast universal RNA-seq aligner. *Bioinformatics*, *29*(1), 15-21. https://doi.org/10.1093/bioinformatics/bts635

Doukani, K., Selles, A. S. M., Bouhenni, H., Chafaa, M., & Soudani, L. (2022). Chapter4.4 - Carotenoids (Xanthophylls and Carotenes). In S. M. Nabavi & A. S. Silva (Eds.), *Antioxidants Effects in Health* (pp. 279-308). Elsevier. https://doi.org/https://doi.org/10.1016/B978-0-12-819096-8.00044-6

Dzurendova, S., Zimmermann, B., Kohler, A., Reitzel, K., Nielsen, U. G., Dupuy--Galet, B. X., Leivers, S., Horn, S. J., & Shapaval, V. (2021). Calcium Affects Polyphosphate and Lipid Accumulation in Mucoromycota Fungi. *Journal of Fungi*, *7*(4), 300. https://www.mdpi.com/2309-608X/7/4/300

Dzurendova, S., Zimmermann, B., Tafintseva, V., Kohler, A., Horn, S. J., & Shapaval, V. (2020). Metal and Phosphate Ions Show Remarkable Influence on the Biomass Production and Lipid Accumulation in Oleaginous Mucor circinelloides. *J Fungi (Basel)*, *6*(4). https://doi.org/10.3390/jof6040260

Emms, D. M., & Kelly, S. (2019). OrthoFinder: phylogenetic orthology inference for comparative genomics. *Genome Biology*, *20*(1), 238. https://doi.org/10.1186/s13059-019-1832-y

Fazili, A. B. A., Shah, A. M., Zan, X., Naz, T., Nosheen, S., Nazir, Y., Ullah, S., Zhang, H., & Song, Y. (2022). Mucor circinelloides: a model organism for oleaginous fungi and its potential applications in bioactive lipid production. *Microbial Cell Factories*, *21*(1), 29. https://doi.org/10.1186/s12934-022-01758-9

Gauthier, G. M. (2017). Fungal Dimorphism and Virulence: Molecular Mechanisms for Temperature Adaptation, Immune Evasion, and In Vivo Survival. *Mediators Inflamm*, *2017*, 8491383. https://doi.org/10.1155/2017/8491383

Giuraniuc, C. V., Parkin, C., Almeida, M. C., Fricker, M., Shadmani, P., Nye, S., Wehmeier, S., Chawla, S., Bedekovic, T., Lehtovirta-Morley, L., Richards, D., Gow, N. A., & Brand, A. C. (2023). Dynamic calcium-mediated stress response and recovery signatures in the fungal pathogen, <em>Candida albicans</em&gt. *bioRxiv*, 2023.2004.2020.537637. https://doi.org/10.1101/2023.04.20.537637

Gmoser, R., Ferreira, J. A., Lennartsson, P. R., & Taherzadeh, M. J. (2017). Filamentous ascomycetes fungi as a source of natural pigments. *Fungal Biology and Biotechnology*, *4*(1), 4. https://doi.org/10.1186/s40694-017-0033-2

Igreja, W. S., Maia, F. A., Lopes, A. S., & Chisté, R. C. (2021). Biotechnological Production of Carotenoids Using Low Cost-Substrates Is Influenced by Cultivation Parameters: A Review. *Int J Mol Sci*, *22*(16). https://doi.org/10.3390/ijms22168819

Ismaiel, M. M. S., El-Ayouty, Y. M., Said, A. A., & Fathey, H. A. (2018). Transformation of Dunaliella parva with PSY gene: Carotenoids show enhanced antioxidant activity under polyethylene glycol and calcium treatments. *Biocatalysis and Agricultural Biotechnology*, *16*, 378-384. https://doi.org/https://doi.org/10.1016/j.bcab.2018.09.011

Iturriaga, E. A., Velayos, A., & Eslava, A. P. (2000). Structure and function of the genes involved in the biosynthesis of carotenoids in the mucorales. *Biotechnology and Bioprocess Engineering*, *5*(4), 263-274. https://doi.org/10.1007/BF02942183

Kolmogorov, M., Yuan, J., Lin, Y., & Pevzner, P. A. (2019). Assembly of long, error-prone reads using repeat graphs. *Nature Biotechnology*, *37*(5), 540-546. https://doi.org/10.1038/s41587-019-0072-8

Kong, K. W., Khoo, H. E., Prasad, K. N., Ismail, A., Tan, C. P., & Rajab, N. F. (2010). Revealing the power of the natural red pigment lycopene. *Molecules*, *15*(2), 959-987. https://doi.org/10.3390/molecules15020959

Lee, S. C., Billmyre, R. B., Li, A., Carson, S., Sykes, S. M., Huh, E. Y., Mieczkowski, P., Ko, D. C., Cuomo, C. A., & Heitman, J. (2014). Analysis of a food-borne fungal pathogen outbreak: virulence and genome of a Mucor circinelloides isolate from yogurt. *mBio*, *5*(4), e01390-01314. https://doi.org/10.1128/mBio.01390-14

Lee, S. C., Li, A., Calo, S., & Heitman, J. (2013). Calcineurin Plays Key Roles in the Dimorphic Transition and Virulence of the Human Pathogenic Zygomycete Mucor circinelloides. *PLoS Pathogens*, *9*(9), e1003625. https://doi.org/10.1371/journal.ppat.1003625

Li, C., Swofford, C. A., & Sinskey, A. J. (2020). Modular engineering for microbial production of carotenoids. *Metabolic Engineering Communications*, *10*, e00118. https://doi.org/https://doi.org/10.1016/j.mec.2019.e00118

Li, S., Yang, J., Mohamed, H., Wang, X., Pang, S., Wu, C., López-García, S., & Song, Y. (2022). Identification and Functional Characterization of Adenosine Deaminase in Mucor circinelloides: A Novel Potential Regulator of Nitrogen Utilization and Lipid Biosynthesis. *Journal of Fungi*, *8*(8), 774. https://www.mdpi.com/2309-608X/8/8/774

Love, M. I., Huber, W., & Anders, S. (2014). Moderated estimation of fold change and dispersion for RNA-seq data with DESeq2. *Genome Biology*, *15*(12), 550. https://doi.org/10.1186/s13059-014-0550-8

Manni, M., Berkeley, M. R., Seppey, M., Simão, F. A., & Zdobnov, E. M. (2021). BUSCO Update: Novel and Streamlined Workflows along with Broader and Deeper

Phylogenetic Coverage for Scoring of Eukaryotic, Prokaryotic, and Viral Genomes. *Molecular Biology and Evolution*, *38*(10), 4647-4654. https://doi.org/10.1093/molbev/msab199

Moreau, R. A. (1987). Calcium-Binding Proteins in Fungi and Higher Plants. *Journal of Dairy Science*, *70*(7), 1504-1512. https://doi.org/https://doi.org/10.3168/jds.S0022-0302(87)80174-1

Mosqueda-Cano, G., & Gutiérrez-Corona, J. F. (1995). Environmental and developmental regulation of carotenogenesis in the dimorphic fungus Mucor rouxii. *Current Microbiology*, *31*(3), 141-145. https://doi.org/10.1007/BF00293544

Nagy, G., Szebenyi, C., Csernetics, Á., Vaz, A. G., Tóth, E. J., Vágvölgyi, C., & Papp, T. (2017). Development of a plasmid free CRISPR-Cas9 system for the genetic modification of Mucor circinelloides. *Scientific Reports*, *7*(1), 16800. https://doi.org/10.1038/s41598-017-17118-2

Navarro, E., Lorca-Pascual, J. M., Quiles-Rosillo, M. D., Nicolás, F. E., Garre, V., Torres-Martínez, S., & Ruiz-Vázquez, R. M. (2001). A negative regulator of light-inducible carotenogenesis in Mucor circinelloides. *Mol Genet Genomics*, *266*(3), 463-470. https://doi.org/10.1007/s004380100558

Naz, T., Nosheen, S., Li, S., Nazir, Y., Mustafa, K., Liu, Q., Garre, V., & Song, Y. (2020). Comparative Analysis of β-Carotene Production by Mucor circinelloides Strains CBS 277.49 and WJ11 under Light and Dark Conditions. *Metabolites*, *10*(1). https://doi.org/10.3390/metabo10010038

Nelis, H. J., & De Leenheer, A. P. (1991). Microbial sources of carotenoid pigments used in foods and feeds. *Journal of Applied Bacteriology*, *70*(3), 181-191. https://doi.org/https://doi.org/10.1111/j.1365-2672.1991.tb02922.x

Patro, R., Duggal, G., Love, M. I., Irizarry, R. A., & Kingsford, C. (2017). Salmon provides fast and bias-aware quantification of transcript expression. *Nat Methods*, *14*(4), 417-419. https://doi.org/10.1038/nmeth.4197

Powers-Fletcher, M. V., Kendall, B. A., Griffin, A. T., & Hanson, K. E. (2016). Filamentous Fungi. *Microbiology Spectrum*, *4*(3), 4.3.23. https://doi.org/doi:10.1128/microbiolspec.DMIH2-0002-2015

Rhie, A., Walenz, B. P., Koren, S., & Phillippy, A. M. (2020). Merqury: reference-free quality, completeness, and phasing assessment for genome assemblies. *Genome Biology*, *21*(1), 245. https://doi.org/10.1186/s13059-020-02134-9

Roy, A., Kumar, A., Baruah, D., & Tamuli, R. (2021). Calcium signaling is involved in diverse cellular processes in fungi. *Mycology*, *12*(1), 10-24. https://doi.org/10.1080/21501203.2020.1785962

Sandra, R. P.-S., Gabriela, S. S., Jazmina, C. R. A., Helen, F. L., & Rita, C. R. G. (2017). Production of Melanin Pigment by Fungi and Its Biotechnological Applications. In B. Miroslav (Ed.), *Melanin* (pp. Ch. 4). IntechOpen. https://doi.org/10.5772/67375

Saraswati, T. E., Setiawan, U. H., Ihsan, M. R., Isnaeni, I., & Herbani, Y. (2019). The Study of the Optical Properties of C60 Fullerene in Different Organic Solvents. *Open Chemistry*, *17*(1), 1198-1212. https://doi.org/doi:10.1515/chem-2019-0117

Silva, F., Torres-Martínez, S., & Garre, V. (2006). Distinct white collar-1 genes control specific light responses in Mucor circinelloides. *Molecular Microbiology*, *61*(4), 1023-1037. https://doi.org/https://doi.org/10.1111/j.1365-2958.2006.05291.x

Szebenyi, C., Gu, Y., Gebremariam, T., Kocsubé, S., Kiss-Vetráb, S., Jáger, O., Patai, R., Spisák, K., Sinka, R., Binder, U., Homa, M., Vágvölgyi, C., Ibrahim, A. S., Nagy, G., & Papp, T. (2023). cotH Genes Are Necessary for Normal Spore Formation and Virulence in Mucor lusitanicus. *mBio*, *14*(1), e03386-03322. https://doi.org/doi:10.1128/mbio.03386-22

Tapiero, H., Townsend, D. M., & Tew, K. D. (2004). The role of carotenoids in the prevention of human pathologies. *Biomed Pharmacother*, *58*(2), 100-110. https://doi.org/10.1016/j.biopha.2003.12.006

Trieu, T. A., Navarro-Mendoza, M. I., Pérez-Arques, C., Sanchis, M., Capilla, J., Navarro-Rodriguez, P., Lopez-Fernandez, L., Torres-Martínez, S., Garre, V., Ruiz-Vázquez,

R. M., & Nicolás, F. E. (2017). RNAi-Based Functional Genomics Identifies New Virulence Determinants in Mucormycosis. *PLoS Pathogens*, *13*(1), e1006150. https://doi.org/10.1371/journal.ppat.1006150

Umeno, D., Tobias, A. V., & Arnold, F. H. (2002). Evolution of the C30 carotenoid synthase CrtM for function in a C40 pathway. *J Bacteriol*, *184*(23), 6690-6699. https://doi.org/10.1128/jb.184.23.6690-6699.2002

Wagner, L., Stielow, J. B., de Hoog, G. S., Bensch, K., Schwartze, V. U., Voigt, K., Alastruey-Izquierdo, A., Kurzai, O., & Walther, G. (2020). A new species concept for the clinically relevant Mucor circinelloides complex. *Persoonia*, *44*, 67-97. https://doi.org/10.3767/persoonia.2020.44.03

Wang, H.-M., To, K.-Y., Lai, H.-M., & Jeng, S.-T. (2016). Modification of flower colour by suppressing β-ring carotene hydroxylase genes in Oncidium. *Plant Biology*, *18*(2), 220-229. https://doi.org/https://doi.org/10.1111/plb.12399

Wozniak, A., Lozano, C., Barahona, S., Niklitschek, M., Marcoleta, A., Alcaíno, J., Sepulveda, D., Baeza, M., & Cifuentes, V. (2011). Differential carotenoid production and gene expression in Xanthophyllomyces dendrorhous grown in a nonfermentable carbon source. *FEMS Yeast Research*, *11*(3), 252-262. https://doi.org/10.1111/j.1567-1364.2010.00711.x

7 Appendix

Appendix 1: GO enrichment upregulated DEGs

YDL240W	YHR206W	YGR027C	YLR185W	YGR009C	YGR192C
YGL216W	YDR352W	YJL053W	YLR143W	YKL135C	YER114C
YLR310C	YKL043W	YPL143W	YNL298W	YKL135C	YDL154W
YBR043C	YBR019C	YLR371W	YGR144W	YNL123W	YDL154W
YIL160C	YMR137C	YBL027W	YHL007C	YJL012C	YDL122W
YBR172C	YMR230W	YJR054W	YJL141C	YDR122W	YHR124W
YBR172C	YNL313C	YGL178W	YJL141C	YDR375C	YEL054C
YDR382W	YIL033C	YCR036W	YEL036C	YKL182W	YFL021W
YLR248W	YBR089C-	YOR086C	YBR191W	YPL249C-	YMR116C
YIL052C	YBR020W	YBR031W	YCR028C	YGR217W	YJL108C
YJL102W	YMR121C	YLR061W	YPL104W	YML016C	YBR046C
YER075C	YDL205C	YLR406C	YDL085W	YIL131C	YLR092W
YHR178W	YBR241C	YOL102C	YJL177W	YER120W	YIL044C
YIR007W	YLR325C	YAL060W	YIL133C	YDR001C	YOR099W
YDR064W	YDL210W	YMR226C	YNL101W	YJR123W	YDR150W
YKL069W	YLR401C	YDR382W	YBR239C	YIL046W	YLR419W
YKR057W	YNL241C	YEL007W	YLR234W	YIL046W	YER074W
YBL061C	YOL127W	YLR319C	YLR234W	YKR009C	YLR371W
YBR151W	YOR369C	YDR017C	YNL217W	YBL049W	YGL096W
YNL178W	YOR096W	YLR307W	YLL029W	YBL049W	YGR144W
YKR080W	YEL054C	YAL067C	YER131W	YCR008W	YHR005C
YNL202W	YOR197W	YJR123W	YKR105C	YKL104C	YMR242C
YKR052C	YDR283C	YJR123W	YOR293W	YBR019C	YPL230W
YOL139C	YDR402C	YLR410W	YGL166W	YKL135C	YDR030C
YOL002C	YLR441C	YGL252C	YIR004W	YBR017C	YDR030C
YHR005C	YJR145C	YAL041W	YHR104W	YNL011C	YGR034W
YHL032C	YJL177W	YOR100C	YBR164C	YDR058C	YLR243W
YPL220W	YNL069C	YBR023C	YPL210C	YDR075W	YPL147W
YKL071W	YBL011W	YBR180W	YNL024C	YOR197W	YDR379W
YDR345C	YOL052C	YOR134W	YPL082C	YFR053C	YKL221W
YDR345C	YOR194C	YPL131W	YNL111C	YPL145C	YHR183W
YIL130W	YNL021W	YGL205W	YOR063W	YPL145C	YNR019W
YLR340W	YOL120C	YKR066C	YFR053C	YER155C	YIL052C
YDL081C	YKR099W	YGL191W	YFR053C	YNL094W	YMR242C
YJR048W	YER126C	YKR093W	YKR093W	YKL141W	YGR055W
YBR180W	YGL123W	YKR093W	YHR008C	YGL073W	YDR032C
YDR481C	YFL027C	YNL154C	YGL209W	YFR031C-	YCR004C
YBR241C	YMR230W	YJL036W	YGR096W	YNL302C	YCR061W
YOL052C	YNR074C	YCL038C	YBL072C	YPL127C	YBR114W
YGL225W	YLL045C	YJL168C	YPR102C	YDL103C	YNL067W

YER074W	YKR088C	YJL168C	YJR040W	YLR371W	YNL067W
YKL192C	YHL015W	YNL240C	YMR116C	YNL083W	YBR126C
YDL210W	YMR166C	YEL064C	YFR031C-	YLR138W	YLR307W
YGL077C	YDR513W	YCR079W	YOL016C	YDR270W	YIL155C
YPL198W	YGL073W	YER129W	YMR121C	YOL127W	YIL033C
YKL006W	YER040W	YKL221W	YGR215W	YGL030W	YDR091C
YER118C	YGR034W	YLR118C	YOL092W	YHR117W	YOL060C
YOR374W	YGR027C	YER141W	YHR179W	YHR114W	YPL143W
YDR036C	YDR083W	YJL137C	YLR348C	YKR050W	YML026C
YBR191W	YER155C	YBL072C	YLR348C	YDR150W	YOR063W
YPL081W	YGR170W	YMR142C	YDL006W	YLR397C	YDR373W
YIL166C	YGL123W	YBR137W	YFR031C-	YDR256C	YHR158C
YJL190C	YPR015C	YKL209C	YGR085C	YOR231W	YPL115C
YFL021W	YMR185W	YIL044C	YNR019W	YOR231W	YML026C
YAL067C	YHR079C	YNR013C	YPL249C-	YOR120W	YGR038W
YJL164C	YHR142W	YBL037W	YPL110C	YOR120W	YPL196W
YLR441C	YKR031C	YML073C	YFR028C	YPL232W	YPL196W
YDL083C	YCR044C	YBR222C	YLR191W	YLR264W	YNL096C
YJL134W	YPL090C	YJL208C	YGL059W	YGR149W	YER051W
YCR031C	YHR007C	YER062C	YHL015W	YGR034W	YBL087C
YHR010W	YPR015C	YLR289W	YDR523C	YBR220C	YAL041W
YOR127W	YCR061W	YCR031C	YBR106W	YOL115W	YNR047W
YKR057W	YJR001W	YML004C	YOR022C	YLR061W	YNR047W
YLR185W	YER131W	YMR228W	YGL205W	YOL092W	YMR261C
YPR091C	YNL168C	YGL114W	YER131W	YJL094C	YLR244C
YNR017W	YLR441C	YPL249C	YFR022W	YDR025W	YKL146W
YMR226C	YKR093W	YHR010W	YPL029W	YDL103C	YML026C
YEL046C	YGL030W	YGR214W	YFL021W	YIL031W	YNL302C
YLR092W	YGL030W	YKL085W	YDR447C	YBR176W	YGL023C
YIL124W	YML073C	YDL083C	YML072C	YPR155C	YPL249C
YMR226C	YGR003W	YIL113W	YKL043W	YJL164C	YMR142C
YEL054C	YBR239C	YGR118W	YDR236C	YHR142W	YNL178W
YDR111C	YPR086W	YGL073W	YBR191W	YDR345C	YOR233W
YJR094W-	YGL103W	YGL073W	YNL271C	YHR021C	YCL035C
YER049W	YBR222C	YNL191W	YHR073W	YNL267W	YNL047C
YDL036C	YDR032C	YNL068C	YPL143W	YNL267W	YJL212C
YOL158C	YMR140W	YBL092W	YNR017W	YML008C	YCR105W
YHL001W	YOL120C	YGR046W	YBR256C	YBL007C	YNR029C
YNL064C	YDL210W	YOR262W	YOR089C	YBL061C	YFL050C
YDL083C	YPR102C	YKR084C	YDR477W	YHL033C	YHR090C
YGR032W	YKL020C	YKR084C	YDL103C	YMR242C	YKR094C
YMR043W	YGL073W	YDL191W	YBL092W	YBR008C	YKR094C
YNL106C	YHR206W	YGR100W	YNL271C	YIL047C	

Appendix 2: GO enrichment downregulated DEGs

YDR410C	YDR127W	YFL050C	YAL023C	YOR125C	YJL060W
YDR036C	YER179W	YNR043W	YPR028W	YMR297W	YDR011W
YJL163C	YGL011C	YIL107C	YHL007C	YMR297W	YNR016C
YDL003W	YJL034W	YKL209C	YOL071W	YDR036C	YHL004W
YKL059C	YFL030W	YBL061C	YOR046C	YJR104C	YBR159W
YNR030W	YFL030W	YKL016C	YDR402C	YOR335C	YNL004W
YIL034C	YHR178W	YOL158C	YDL097C	YBR249C	YEL064C
YMR022W	YHR178W	YKL209C	YJR121W	YPL154C	YOR181W
YJL096W	YMR226C	YHR071W	YPR013C	YHL027W	YML060W
YAL005C	YGR037C	YGR038W	YPR108W	YGR185C	YOR157C
YJL088W	YBR023C	YDR302W	YDL097C	YFR050C	YKR001C
YHR104W	YDL178W	YKL190W	YOR250C	YLR128W	YER103W
YER094C	YJL167W	YBR241C	YGL048C	YMR140W	YLR304C
YPL154C	YMR076C	YPL036W	YER119C	YML078W	YOR067C
YPL154C	YJL074C	YDL056W	YER119C	YOL012C	YBL058W
YDR144C	YLR084C	YGR243W	YHR183W	YJL206C	YKL060C
YKL209C	YCL009C	YPL094C	YOL098C	YHL007C	YIL075C
YJR109C	YNL030W	YOR281C	YFR015C	YHR027C	YIL075C
YPL123C	YDR006C	YBR290W	YNL273W	YKL160W	YJL055W
YER165W	YNL279W	YDR167W	YDL128W	YEL002C	YML085C
YDR155C	YJL041W	YMR296C	YJR149W	YJL111W	YDR205W
YER141W	YPL151C	YER012W	YOR303W	YPL240C	YDL240W
YJL186W	YNL049C	YDL216C	YNL316C	YPR189W	YIL118W
YOL060C	YMR023C	YHR179W	YML086C	YNL289W	YJR139C
YLR275W	YDL029W	YJL012C	YDL108W	YJR119C	YOL058W
YIL026C	YDL029W	YOL140W	YPL162C	YER142C	YKL013C
YNL048W	YBR088C	YOR275C	YER065C	YDR486C	YDR390C
YNL032W	YPR004C	YOR362C	YER065C	YJR070C	YDR390C
YER081W	YOR149C	YOR317W	YER065C	YMR210W	YLR109W
YFL039C	YKL087C	YKR003W	YOR099W	YDR080W	YFR037C
YIL125W	YJL115W	YGR194C	YER021W	YGL083W	YMR071C
YER052C	YGR253C	YER154W	YNR013C	YDL231C	YHL007C
YER165W	YGL201C	YKR048C	YLR046C	YGL059W	YOR238W
YJR126C	YOR374W	YER048C	YDL015C	YLR046C	YJL100W
YGR028W	YLR239C	YDR293C	YJR013W	YOR033C	YOR288C
YMR096W	YOR332W	YBR196C	YDR337W	YBR011C	YNL197C
YEL056W	YHR171W	YFR022W	YFL018C	YBL008W	YNL197C
YNL011C	YGL006W	YJR064W	YMR284W	YFL008W	YPR113W
YNL334C	YNR015W	YDR244W	YMR285C	YBL095W	YPR023C
YBL035C	YKL007W	YDR338C	YCL057W	YIR023W	YHR128W
YLR307W	YIL160C	YPL051W	YFR037C	YER070W	YCR094W
YKL157W	YJR001W	YDR122W	YJL194W	YDR388W	YBL099W

YOR299W	YOR259C	YBR087W	YBL082C	YPR108W	YPL259C
YER069W	YHR200W	YGR207C	YNR058W	YDR132C	YKL148C
YPL004C	YBR003W	YPR058W	YFR010W	YBR166C	YBR222C
YHL007C	YOL049W	YNL326C	YGL252C	YOR271C	YOR336W
YDR092W	YOR351C	YIL004C	YLR001C	YML021C	YHR123W
YLR328W	YGL018C	YBR135W	YLL048C	YBR208C	YJL121C
YHR147C	YMR034C	YMR075W	YMR093W	YPL069C	YHR030C
YKL211C	YKL213C	YJR068W	YMR093W	YBR153W	YHR019C
YML020W	YJL026W	YLR370C	YDR212W	YOR288C	YNR070W
YBL038W	YGR257C	YDL128W	YER107C	YDL101C	YBR114W
YJR060W	YGR282C	YOR217W	YPL162C	YKR009C	YLR177W
YHR188C	YBR038W	YEL056W	YLR231C	YOR175C	YGL167C
YBR010W	YDL236W	YBR180W	YCL030C	YGL208W	YER114C
YBL013W	YKL126W	YBR008C	YOL139C	YDL147W	YBL023C
YCL039W	YDR170C	YML069W	YBR056W	YAL021C	YOR168W
YCR094W	YEL032W	YML092C	YCR015C	YJR105W	YIR008C
YNL106C	YPL162C	YPL262W	YNL072W	YKL045W	YBR115C
YGR264C	YML126C	YNL217W	YGR257C	YDL164C	YCR065W
YGR157W	YKL207W	YNL217W	YOL107W	YER086W	YNL290W
YDL007W	YCL045C	YJR107W	YFR004W	YFL039C	YNR050C
YBL055C	YGL019W	YNL287W	YOR304W	YJL036W	YMR129W
YKL071W	YGL019W	YPL249C	YJL168C	YJL072C	YJR006W
YGR178C	YGR135W	YHL031C	YDR436W	YMR062C	YPL088W
YPR135W	YHR120W	YJL002C	YGL065C	YDL102W	
YJL031C	YHR120W	YOR270C	YNL102W	YJL154C	
YDR221W	YJL012C	YER007W	YGL156W	YFR015C	
YBR222C	YOL038W	YKR070W	YML072C	YBR010W	
YOR033C	YDL142C	YDR035W	YBR003W	YDR224C	

Norges miljø- og biovitenskapelige universitet
Noregs miljø- og biovitskapelege universitet
Norwegian University of Life Sciences

Postboks 5003
NO-1432 Ås
Norway